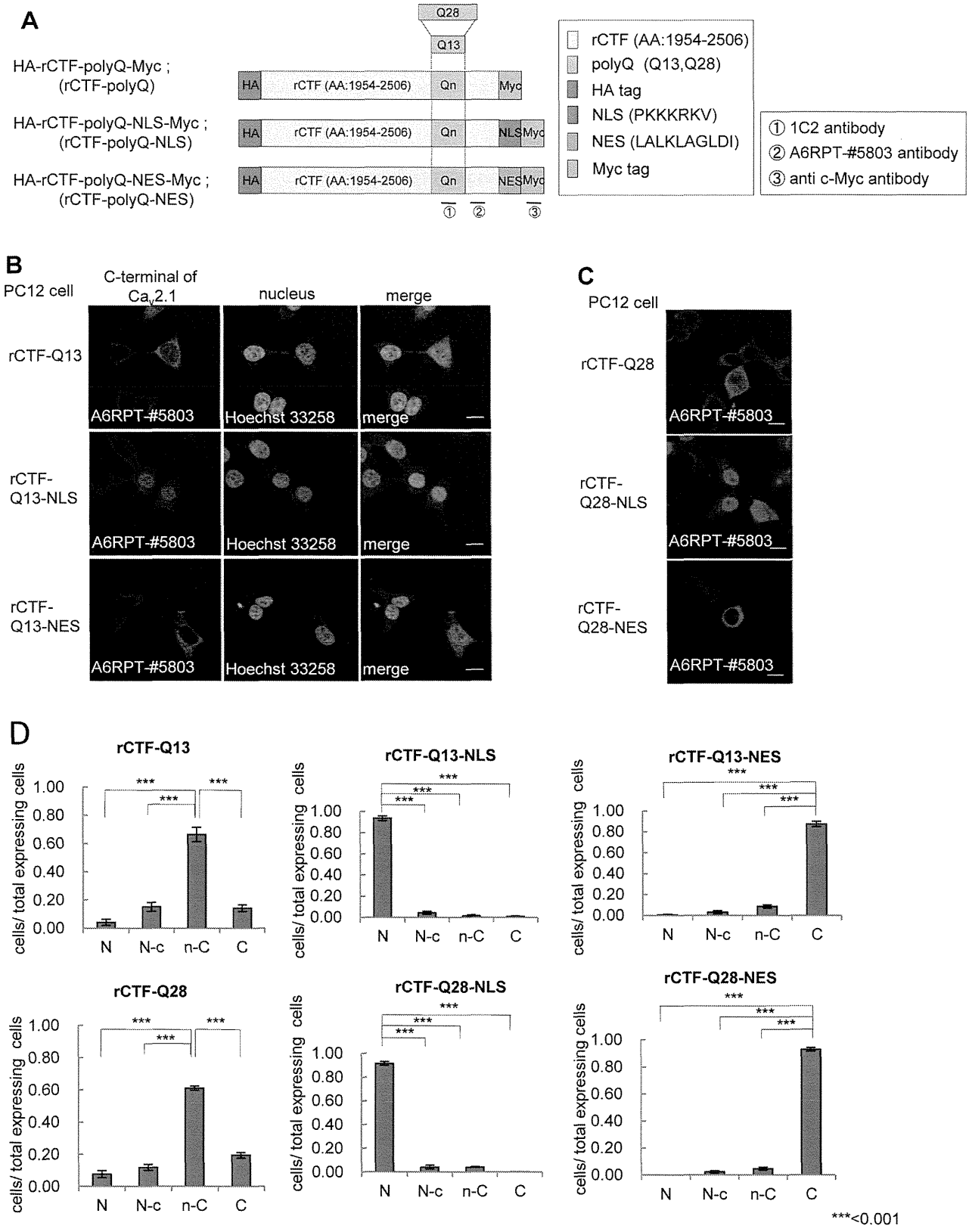

Figure 1. Localization signals efficiently change the intracellular location of CTF. (A) Recombinant $Ca_v2.1$ C-terminal fragment (rCTF)s used in this study. Definition of rCTF (amino acid(AA) #1954–2506 in $Ca_v2.1$ [GenBank AB035726] [18]), artificial nuclear localization or export signals (NLS or NES), two different polyglutamine (Qn) (Q13; Q28) and recognition sites of three different antibodies (1C2 against expanded polyQ, A6RPT-#5803 against $Ca_v2.1$ CTF, c-Myc antibody against Myc-tag) are shown. (B) The rCTF-Q13 is predominantly expressed in the cytoplasm of PC12 cells. The NLS and NES efficiently localize the tagged rCTF to the designed location [A6RPT-#5803 antibody (red), Hoechst 33258 (blue)] (scale bar: 10 μm). (C) The

NLS and NES efficiently shift rCTFs with expanded polyQ (Q28) into the nucleus and cytoplasm respectively (scale bars: 10 μm). (D) The proportion of the subcellular localization in each rCTF expressed. The rCTF-polyQ is predominantly, though not exclusively, expressed in the cytoplasm of PC12 cells. The localization signals change subcellular localization of rCTFs-polyQ effectively. (N; the cells expressing rCTF exclusively in the nucleus; N-c: the cells expressing rCTF predominantly in the nucleus than in the cytoplasm; n-C: the cells expressing rCTF predominantly in the cytoplasm than in the nucleus; C: the cells expressing rCTF exclusively in the cytoplasm) (For D: ***:$p<0.001$;ANOVA. Error bars indicate ± SEM.).
doi:10.1371/journal.pone.0050121.g001

started to be detected on Day4 and become conspicuous on Day6 (Figure 2E). In stable rCTF-Q13-NES cells, the rCTF aggregates were observed only with A6RPT-#5803 but not with 1C2. Because no aggregates are detected by A6RPT-#5803 in normal human brains, the stable PC12 cells expressing rCTF-Q13-NES can be considered as an exaggerated cell model for normal CTF. On the other hand, those expressing rCTF-Q28-NES recapitulated SCA6 aggregates in human Purkinje cells, showing A6RPT-#5803 and 1C2 double-positive aggregates [18].

Cytoplasmic expression of CTF triggered cell death with aggregate formation

We next asked whether the CTF is more toxic in the nucleus than in the cytoplasm, as in other polyQ diseases [2]. To address this question, we transiently over-expressed rCTF-polyQ-NLS or rCTF-polyQ-NES in HEK293T cells, and measured cell death by lactate dehydrogenase (LDH) assay at 72 hours after transfection. Surprisingly, we found that the rCTF-polyQ-NES showed stronger toxicity than the rCTF-polyQ-NLS, regardless of the polyQ lengths (Figure 3A). This is striking, as most proteins

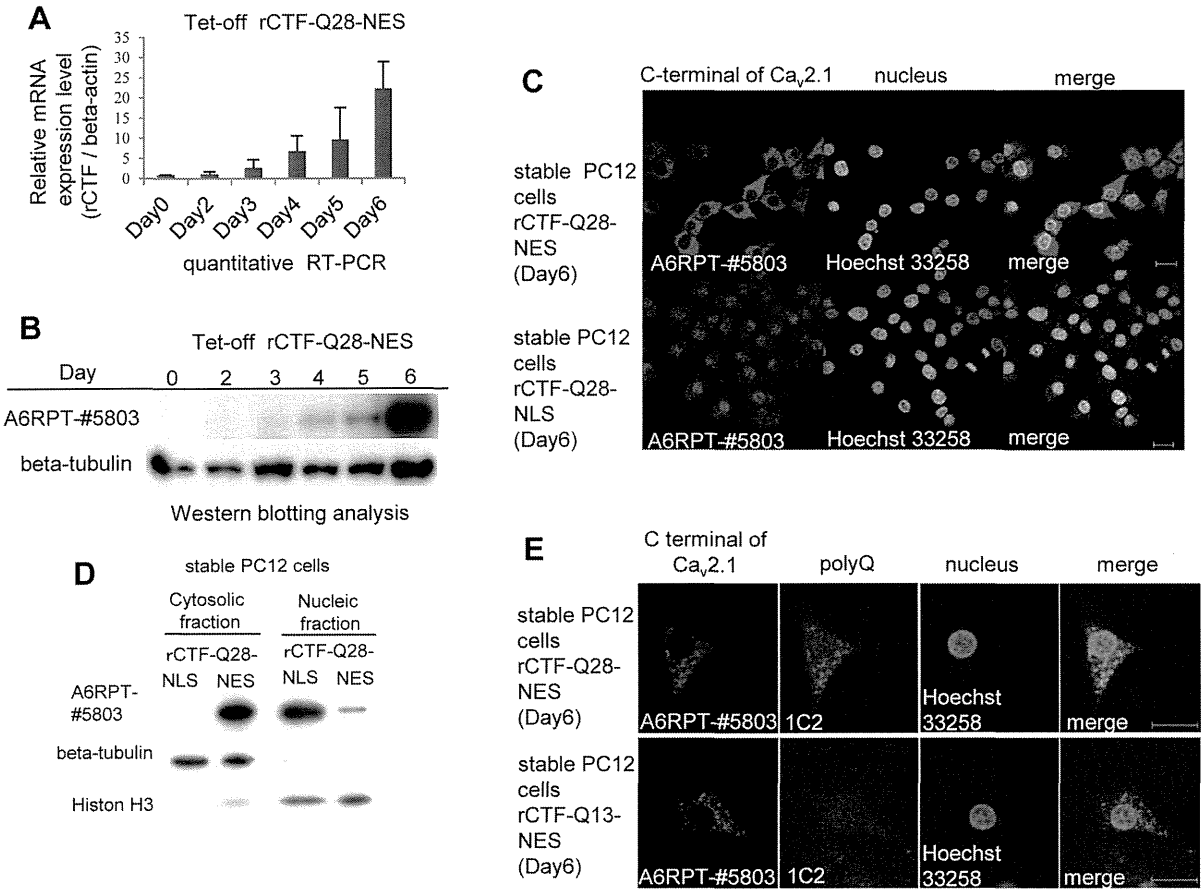

Figure 2. Characterization of inducible PC12 cells stably expressing rCTFs. Only the cell lines expressing rCTF-Q28-NES, rCTF-Q28-NLS and rCTF-Q13-NES are shown here (*Other cells are shown upon request*). (A) A timeline of rCTF expression in PC12 cells stably expressing rCTF-Q28-NES by quantitative real-time PCR (qRT-PCR). The rCTF mRNA level starts to be detected inDay3 and gradually increases with a time-dependent manner. The beta-actin expression level was used as an internal control. (B) A timeline of rCTF expression in PC12 cells stably expressing rCTF-Q28-NES by Western blot using the A6RPT-#5803 antibody. Protein expression starts to be detected on the fourth day after the Dox removal ("Day4") and reaches abundant level in Day6. Anti beta-tubulin antibody was used as internal control. (C) Immunofluorescence cytochemistry in Day6 stable PC12 cell lines expressing rCTF-Q28-NES (upper row) and rCTF-Q28-NLS (lower row). The NES-tag faithfully anchored rCTF to the cytoplasm, whereas the NLS-tag efficiently directed rCTF to the nucleus. (D) Western blot analysis on protein extracts from stable cell lines expressing rCTF-Q28-NLS and rCTF-Q28-NES confirming efficient intracellular localizations (A6RPT-#5803: anti-$Ca_V2.1$CTF, beta-tubulin: a cytoplasmic protein marker, Histone H3: a nuclear protein marker). (E) Immunofluorescence cytochemistry in Day6 stable PC12 cell lines expressing rCTF-Q28-NES (upper row) and rCTF-Q13-NES (lower row). In PC12 cells expressing rCTF-Q28-NES, cytoplasmic aggregates are detected by both A6RPT-#5803 and 1C2. In rCTF-Q13-NES cells, rCTF-aggregates are recognized by the anti-$Ca_V2.1$ antibody A6RPT-#5803, but not by 1C2, a monoclonal antibody specific for expanded polyQ. (For C&E, scale bars: 10 μm).
doi:10.1371/journal.pone.0050121.g002

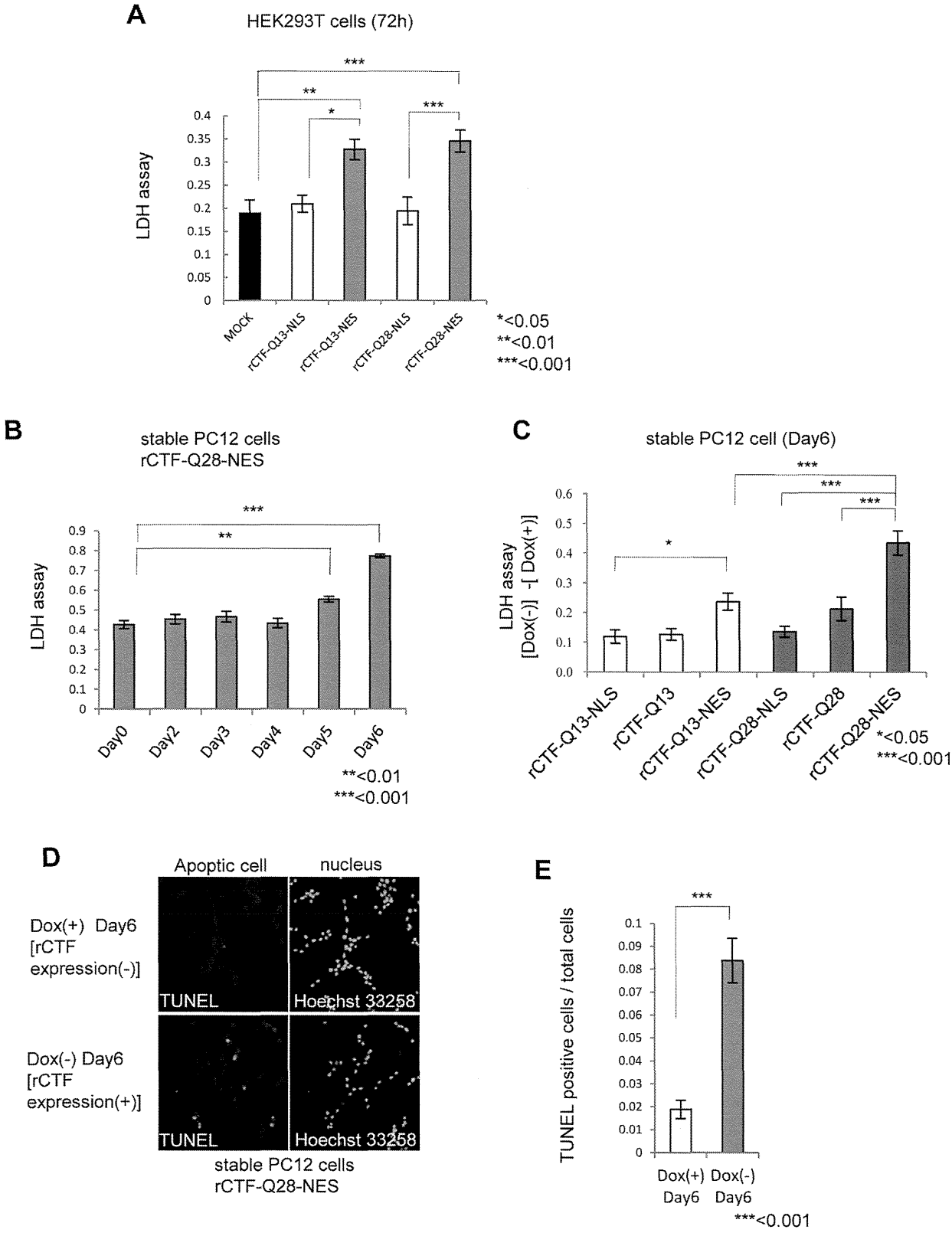

Figure 3. The rCTF is toxic to cells when expressed in the cytoplasm. (A) Cell death in transiently over-expressed HEK293T cells assessed by LDH level at 72 hours after transfection. The rCTF-polyQ-NES exhibits stronger cytotoxicity than rCTF-polyQ-NLS. (B) Time course of cell death in inducible rCTF-Q28-NES PC12 cell line. Cell toxicity is detected from Day5 and become prominent in Day6. (C) The cell death at Day6 compared in 6 inducible PC12 cell lines (rCTF-Q13, rCTF-Q13-NLS, rCTF-Q13-NES, rCTF-Q28, rCTF-Q28-NLS, rCTF-Q28-NES). The cell line expressing rCTF-Q28-NES exerts the strongest cell death. Y-axis shows differences of LDH values between (Dox(−)) and (Dox(+)) states. Cells do not show obvious cell death in Dox(+) states. (D&E) TUNEL positive cells are dramatically increased when doxycyclin is removed (Dox(−)). Eight randomly selected microscope fields

were counted for TUNEL positive cells and total cell numbers. (For A to C and E: *: p<0.05; **: p<0.01; ***:p<0.001;ANOVA for A to C. Mann-Whitney's U test for E. Error bars indicate ± SEM.).
doi:10.1371/journal.pone.0050121.g003

causing polyQ diseases show dramatic cell death when they are expressed in the nucleus.

We then compared the cell toxicity for the period after the Dox removal. In the inducible stable PC12 cell line expressing the rCTF-Q28-NES, we found that the cell death measured by LDH assay started to appear on Day5, and become prominent on Day6 (Figure 3B). We also found the cell death is not seen when the Dox is kept in the media, confirming that the cell death is induced by the rCTF expression in the cytoplasm. Based on these results, we compared cell death at Day6 in the 6 stable PC12 cell lines. In a manner consistent with results from transient expression in HEK293T cells, we found that the stable PC12 cells expressing rCTF-polyQ(Q13, Q28)-NES exerted stronger toxicity than rCTF-polyQ(Q13, Q28) or rCTF-polyQ(Q13, Q28)-NLS (Figure 3C). Importantly, we also found that the PC12 cells expressing rCTF-Q28-NES revealed the strongest toxicity among the 6 cell lines. This is an intriguing finding demonstrating that such a small polyQ repeat, the length that corresponds to a normal repeat in other polyQ diseases, exerts toxicity in the cytoplasm of cultured cells. The cell death was compatible with apoptosis and showed a significant increase of TUNEL (TdT-mediated dUTP-biotin nick end labeling)-positive cells (Figure 3D & 3E).

The cytoplasmic $Ca_v2.1$-CTF aggregates co-localize with CREB and phosphorylated(p)-CREB resulting in reductions of CREB/p-CREB in the nuclei

In other polyQ diseases such as HD, one of the underlying mechanisms for suppressing CREB-dependent transcription is the sequestration of CREB-binding protein (CBP) by the aggregations of mutant proteins within the nuclei [22–25]. However, it is not known if this is also the case in SCA6. To clarify whether and how the CTF suppresses CREB-dependent transcription, we analyzed localizations of rCTF, CREB and phosphorylated-CREB (p-CREB), the active form of CREB, in PC12 cell models. While the immunoreactivities for CREB and p-CREB were both strong in the nuclei, they were very weak in the cytoplasm of non-transfected PC12 cells (Figure 4A). On the other hand, in PC12 cells transiently expressing rCTF-Q28-NES, we found that the cytoplasmic rCTF aggregates co-localized with both CREB and p-CREB demonstrating focally strong immunoreactivities for these proteins (Figure 4B). Similar co-localizations were also observed both for CREB and p-CREB with rCTF aggregates in the stable PC12 cell lines expressing rCTF-Q28-NES in contrast to the control Dox(+) cells (Figure 4C & 4D). When rCTF-Q13-NES was transiently over-expressed in PC12 cells, CREB and p-CREB also co-localized with rCTF aggregates in the cytoplasm (Figure S3). These results suggested to us that the rCTF expression in the cytoplasm indeed alters intracellular distribution of CREB and p-CREB irrespective of the polyQ length.

We also examined whether the formation of cytoplasmic rCTF aggregates influence the quantity of CREB and p-CREB in the nucleus. By Western blot analysis, we found that they were both decreased when the rCTF was expressed in the cytoplasm (Figure 4E). Surprisingly, the reductions of CREB and p-CREB in the nucleus were not observed when the rCTF was expressed directly in the nucleus. Therefore, over-expressing the rCTF in the cytoplasm leads to the reductions of CREB and p-CREB in the nuclei, possibly by retaining them in the cytoplasm through their co-localization with the CTF aggregates. This also suggests that the cytoplasmic CTF aggregates cause the repression of the CREB-dependent transcription through abnormal intracellular trafficking of CREB.

CREB co-localized with cytoplasmic aggregates in the human SCA6 Purkinje cells

We finally examined whether the CREB co-localizes with $Ca_v2.1$ microscopic aggregates in SCA6 Purkinje cells. Although CREB expression was seen in the nuclei of cultured cells, the immunoreactivity against CREB was present but weak and homogeneous in the neuronal cytoplasm in control human Purkinje cells (Figure 5A). This would indicate species or cellular differences in the immunoreactivity against the antibody we used. In SCA6 human Purkinje cells, CREB immunoreactivity was also seen expressed in the cytoplasm. However, granular or thread-like CREB-immunoreactive structures were frequently observed in the cytoplasm of SCA6 Purkinje cells (Figure 5B). When these structures were counted, we observed that SCA6 Purkinje cells show a higher number of CREB-immunoreactive structures than controls (Figure 5 C). We next examined the relationship between the CREB and 1C2-immunoreactive $Ca_v2.1$ aggregates in the SCA6 Purkinje cells by double immunofluorescence technique. We found that the 1C2-immunoreactive microscopic polyQ aggregates in the cytoplasm of SCA6 Purkinje cells indeed co-localize with CREB (Figure 5D). Among the remaining Purkinje cells in the three SCA6 cerebella, we found that 50% of such Purkinje cells had the co-localization of CREB and $Ca_v2.1$ aggregates. As there are no $Ca_v2.1$ aggregates in control Purkinje cells, such co-localization is specific to SCA6 Purkinje cells (Figure 5 E). Also, this co-localization mimics what we observed in cultured cells, suggesting that altered intracellular trafficking of CREB takes place in human SCA6 Purkinje cell as well.

Discussion

Molecular genetics of SCA6 are characterized by two main features; namely, 1) a small polyQ expansion (normal range 4–19 repeat *vs* SCA6 20–33 repeat) that falls within a normal range of other polyQ diseases (usually more than 35 repeat in other polyQ diseases), and 2) the cytoplasmic localization of aggregations which contrasts with nuclear localization in other polyQ diseases [2,16,17]. It should be noted that nuclear aggregates were seen in SCA6 Purkinje cells in a very small amount, though cytoplasmic aggregations are far dominant in both immunohistochemical and Western blotting observations [18]. Thus, it remained to be clarified whether cytoplasmic aggregates are more toxic than nuclear ones, or *vice versa* as in other polyQ diseases. To define which location of the CTF is more toxic, and also to elucidate the mechanisms of its toxicity, we developed cell models expressing rCTF tagged with either NLS or NES. These signals faithfully targeted the rCTF to the aimed intracellular cites (cytoplasm or nucleus). We here demonstrate that the rCTF-Q13 and -Q28 both consistently show toxicity in cultured HEK293T and PC12 cells when the rCTFs are expressed in the cytoplasm. On the other hand, neither rCTF-Q13 nor rCTF-Q28 showed obvious toxicity when expressed in the nucleus. Furthermore, the toxicity exerted by rCTF-Q28-NES was more profound than that of rCTF-Q13-NES, an important observation supporting the fundamental idea that SCA6 complies with the general rule of polyQ-length dependent toxicity in all polyQ diseases. Taking these observations

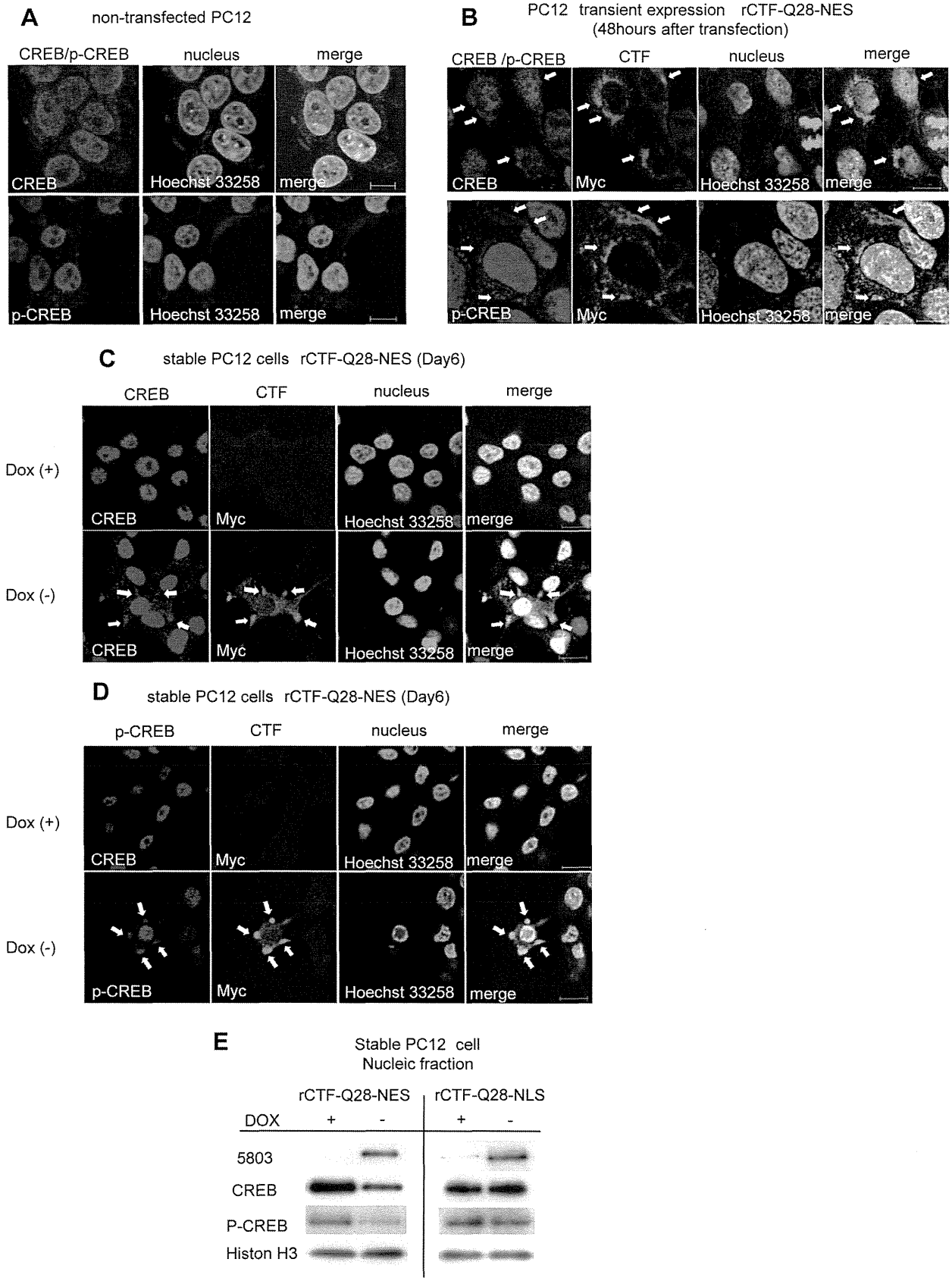

Figure 4. CREB co-localizes with intracytoplasmic CTF aggregates and quantity of CREB is decreased in cultured cell model. (A) In non-transfected PC12 cells, CREB and p-CREB-immunofluorescence labeling is strong in the nucleus, while the cytoplasm shows only weak and diffuse immunofluorescence. (B) In PC12 cells over-expressing rCTF-Q28-NES, the cytoplasmic CTF aggregates co-localize with CREB (*upper row*) and

p-CREB (*lower row*), showing focally strong immunofluorescence in their cell bodies (arrows). (C&D) In contrast to the Dox(+) stable PC12 cells (upper row in C&D), co-localizations of CREB (*lower row in C*) or p-CREB (lower row in D) with cytoplasmic aggregates are also observed in Dox(−) stable PC12 cells expressing rCTF-Q28-NES (arrows). (E) The quantities of CREB and p-CREB in the nucleus were both decreased when the rCTF was expressed in the cytoplasm, but not so when the rCTF was targeted in the nucleus. (For A-D: scale bars: 10 μm).
doi:10.1371/journal.pone.0050121.g004

together, it seems rational to consider that important cascades in SCA6 pathogenesis occur in the cytoplasm of CTF-expressing cells, such as Purkinje cells.

Then how does the CTF cause cell death? Although this is still an open question, we here showed that the cytoplasmic overexpression of rCTF resulted in the altered intracellular distributions of CREB and p-CREB. The CREB and p-CREB both co-localized with $Ca_v2.1$-CTF aggregates in the cytoplasm, and the amount of CREB and p-CREB were both reduced in the nuclei of cultured cells. Furthermore, co-localization of CREB and cytoplasmic $Ca_v2.1$ aggregates was confirmed in human SCA6 Purkinje cells, suggesting that the suppression of CREB-mediated transcription takes place in SCA6 Purkinje cells. Indeed, we recently found that the brain derived neurotrophic factor (BDNF) mRNA, which is regulated by the CREB-mediated transcription, is reduced in SCA6 human cerebellum [26]. It is also important to note that the CREB and p-CREB were not reduced even when the rCTF was over-expressed in the nuclei by tagging the rCTF with NLS. Although the present observation is strikingly different than with other polyQ diseases, in which suppression of CREB-transcription is seen by nuclear localizations of mutated proteins [23,24,27], it should be noted that polyQ-aggregates are also seen in the cytoplasm in other polyQ diseases such as HD [28] and MJD [13], raising a hypothesis that CREB-transcriptional repression may be further enhanced by the formation of protein aggregates in the cytoplasm. It has been shown that the CREB is transported from axons to cell body [29], and translocated from the cytoplasm to the nucleus [30,31]. This retrograde trafficking has been claimed to be important for neurons to survive. Thus, it may be possible that the cytoplasmic protein aggregates can affect neuronal survival by trapping the CREB in the cytoplasm resulting in the reductions of the nuclear CREB and pCREB levels. Interestingly, the CREB-related transcription is suppressed in Parkinson's disease by the formation of p-CREB aggregates in the neuronal cytoplasm [31]. However, many issues remain unsolved concerning the link between the $Ca_v2.1$ with expanded polyQ and the suppression of the CREB-related transcription. For example, it is not known whether the CTF could directly bind CREB/pCREB, as we failed to detect direct interactions between rCTF and CREB by co-immunoprecipitation experiments (data not shown). It is thus possible that some other proteins mediate co-localization of $Ca_v2.1$ aggregates and CREB/pCREB. Further studies are needed to elucidate how CREB and p-CREB co-localize with $Ca_v2.1$ aggregates.

Our observation of cytoplasmic toxicity of the CTF is confounded by two previous studies showing rCTF toxicity in the nuclei [19,20], However, as we showed here, tagging rCTF with EGFP may artificially confine the rCTF into the nuclei. It should also be noted that the components of the rCTFs are not exactly the same as the four studies [18–21]: the present study utilized CTF (Amino acids #1954–#2506) [18] which is exactly the same with the one Li et al. used [20], except for the differences in tag proteins. The CTF used by Kordasiewicz HB et al. (Amino acids #2096–#2510) [19]is slightly shorter than ours, and Marquèze-Pouey et al. [21]used a much shorter CTF (corresponding amino acids #2319-C-term of rat $Ca_v2.1$). Of note is that the size of rCTF we used here is very close to the native CTF judging from the result in Western blot [18]. The toxicity when expressed in the cytoplasm is also supported by another study showing that the rCTF with expanded polyQ caused cell death and promoted the CTF to be condensed at the plasma membrane by interacting with myosin IIB [21]. Although the rCTF-Q28-NLS was not obviously toxic in our system, we do not preclude a possibility that the CTF in the nucleus could exert subtle toxicity. Since the CTF is also present in the nucleus in the SCA6 human brains, the true pathogenic mechanisms of SCA6 are predicted to be more complicated than our cellular models. Particularly, we must admit that our cultured cells should have different intracellular conditions and thus should respond differently to various stimuli compared to the Purkinje cells. Nevertheless, we consider that tracking downstream events in each location of CTF would be an important step for exploring the disease mechanism.

In conclusion, we showed that the CTF with a small polyQ expansion is sufficient to cause toxicity when it forms aggregates in the cytoplasm. This was associated with changes in CREB/p-CREB intracellular distribution, and their quantities in the nucleus. A precise understanding of the consequences of intracellular CTF aggregations such as the mechanism of CREB inactivation and the downstream gene expression changes appear important for establishing fundamental therapy of SCA6.

Materials and Methods

Constructs

Recombinant CTF of $Ca_v2.1$ vector (rCTF-polyQ) encoding the C-terminal 553 amino acids (AA) with either 13 or 28 CAG repeats was constructed as previously described [6]. NLS and NES tags were generated from custom oligonucleotides (Sigma-Aldrich Japan, Tokyo, Japan). NLS was derived from SV40 large T antigen (PKKKRKV) and NES was derived from human cAMP-dependent protein kinase inhibitor, alpha form (LALKLAGLDI), and flanked by restriction sites of *Xba*I. The rCTF-polyQ constructs were digested with *Eco*RV and *Pme*I, destroying the *Xba*I restriction site in the multi cloning site. Then, the resulting blunt-end fragment of rCTF-polyQ was ligated into the *Pme*I-digested pcDNA3.1 (Invitrogen, CA, USA). Finally, NLS or NES was cloned into the *Xba*I site of rCTF-polyQ in pcDNA3.1. EGFP fused rCTF vectors were constructed with pEGFP-C2 vectors (Clontech, CA, USA). The rCTF-polyQ constructs were digested with *Bgl*II and *Eco*RV and the resulting fragment of rCTF-polyQ was ligated into EGFP-C2 vector digested with *Bgl*II and *Sma*I in multi cloning site.

Cell culture and transfection of genes-of-interest

Rat adrenal pheochromocytoma PC12 cells and Human embryonic kidney (HEK293T) cells were obtained from American Type Culture Collection (ATCC, VA, USA). PC12 cells were grown in Dulbecco's Modified Eagle's Medium (DMEM) (WAKO, Saitama, Japan) containing 10% horse serum (HS) (GIBCO, Tokyo, Japan), 5% fetal bovine serum (FBS) (GIBCO) and 1% penicillin/streptomycin (PS) (GIBCO) in a humidified atmosphere of 5% CO_2 at 37°C. HEK293T cells were grown in DMEM containing 10% FBS and 1% PS in a humidified atmosphere of 5% CO_2 at 37°C. Cells were transfected using Lipofectamine 2000 (Invitrogen) according to the manufacturer's protocol.

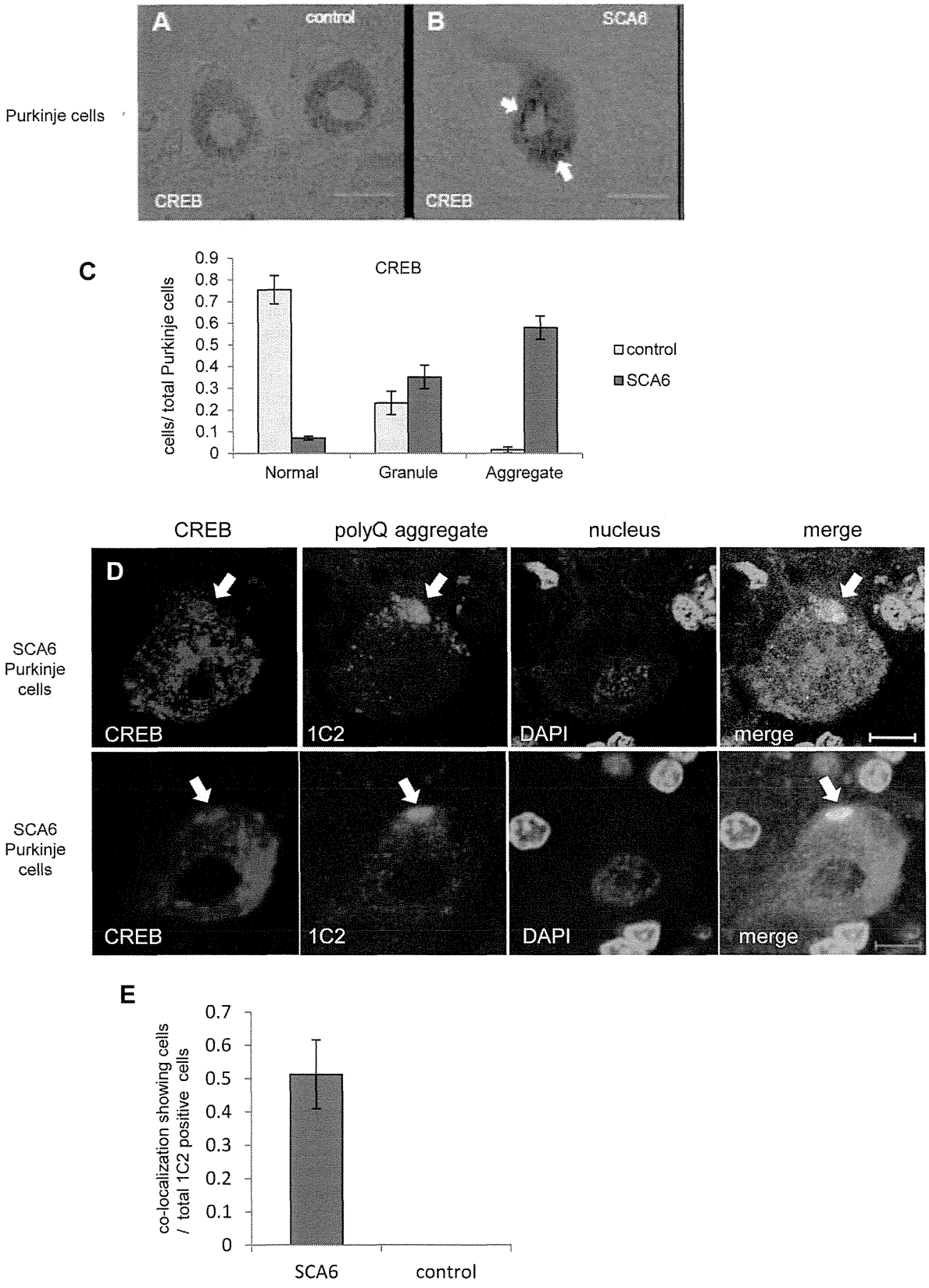

Figure 5. CREB and $Ca_v2.1$ aggregates co-localize in SCA6 human Purkinje cells. (A) In a control brain affected with Parkinson's disease, the immunoreactivity against CREB is present but weak and homogeneous in the neuronal cytoplasm of two Purkinje cells. (B) In SCA6 human Purkinje cells, focally accentuated immunoreactive structures (arrows) are seen in the cytoplasm. (C) In ten control brains, a vast majority of Purkinje cells showed weak and diffuse immunoreactivity for the anti-CREB antibody as demonstrated in the Figure 5 A. In contrast, aggregate-like CREB-immunoreactive structures were seen in the Purkinje cells from three SCA6 cerebella. *Please refer to the Materials and Methods for the detailed*

description on the criteria of CREB-immunoreactivities. (D) On double immunofluorescence analysis using a rabbit polyclonal CREB antibody and 1C2, a mouse monoclonal antibody against expanded polyQ tracts, microscopic $Ca_v2.1$ aggregates in the cytoplasm of the SCA6 Purkinje cells indeed co-localized with CREB (arrows). (For A&B: scale bars: 50 μm; for D&E: scale bar: 10 μm). (E) In three SCA6 cerebella, approximately 50% of Purkinje cells containing 1C2-positive polyQ aggregates in the cytoplasm showed co-localization of the polyQ aggregates and CREB. In contrast, the Purkinje cells in control cerebella did not show 1C2-positive aggregates resulting in no co-localizations.
doi:10.1371/journal.pone.0050121.g005

Generation and culture of inducible PC12 stable cell lines

PC12 Tet-off cell lines (Clontech, CA, USA) were grown in DMEM containing 10% HS, 5% TET-system approved FBS (Clontech), 1% PS and 200 μg/ml G418 (SIGMA, Tokyo, Japan) in a humidified atmosphere of 5% CO_2 at 37°C. Tet-off PC12 cells were transfected with each rCTF vector at 70% confluence using Lipofectamine 2000 (Invitrogen). Positive clones were selected in complete medium containing 200 μg/ml G418 (SIGMA), 200 μg/ml hygromycin (WAKO) and 2 μg/ml doxycycline (Dox) (Clontech). To initiate differentiation, cells were plated on collagen type I-coated plate (IWAKI, Tokyo, Japan) and grown in DMEM containing 1% HS, 1% PS, 200 μg/ml G418, 200 μg/ml hygromycin, 2 μg/ml Dox and 50 ng/ml nerve growth gactor (NGF) 2.5S (Invitrogen, CA, USA).

Immunoblot analysis

The procedure was described previously [18]. Subcellular fractionation was performed with NE-PER Nuclear and Cytoplasmic Extraction Reagents (Pierce, IL, USA).

Cell toxicity and viability analysis

Cell toxicity were assessed by lactate dehydrogenase (LDH) assay with CytoTox 96® Non-Radioactive Cytotoxicity Assay (Promega, WI, USA) and TUNEL assay with DeadEnd™ Fluorometric TUNEL System (Promega). Cell toxicity with LDH assay was calculated using the following formula (experimental LDH release/maximum LDH release).

Immunocytochemistry

The procedure was described previously [6,18]. Either of the following primary antibodies was used; mouse monoclonal anti-c-Myc antibody (diluted with phosphate buffered saline (PBS) into 1:100) (Santa Cruz Biotechnology, CA, USA), rabbit polyclonal A6RPT-#5803 (1:500), rabbit polyclonal anti-CREB antibody (1:500) (Cell Signaling Technology, MA, USA), rabbit polyclonal anti-p-CREB antibody (1:100) (Cell Signaling Technology), mouse monoclonal anti-expanded 1C2 (1:1000)(Millipore, CA, USA). To visualize the anti-p-CREB antibody signal, endogenous PKA was activated by the 10 μM forskolin containing medium for 1 hour before the fixation.

To examine the proportion of cells with a particular subcellular localization of each rCTF, the cells expressing each rCTF were classified into the following four groups and counted in five randomly selected microscope fields: N; the cells expressing rCTF exclusively in the nucleus; N-c: the cells expressing rCTF predominantly in the nucleus than in the cytoplasm; n-C: the cells expressing rCTF predominantly in the cytoplasm than in the nucleus; C: the cells expressing rCTF exclusively in the cytoplasm. The proportion of subcellular localization was calculated using the following formula: total number of cells in each of the four groups/total rCTF expressing cells. The difference was then statistically analyzed using ANOVA.

Immunohistochemistry

Formalin-fixed paraffin-embedded tissue sections of the cerebellar cortex were analyzed. Three SCA6 brains and 10 controls (4 individuals with Parkinson's disease, 2 with amyotrophic lateral sclerosis, 2 with multiple system atrophy, 1 with cerebral infarction, and 1 with SCA31) were investigated. The procedure was described previously [6,13,18]. Either of the following primary antibodies was used; A6RPT-#5803 (diluted in 1:500 concentration with PBS), 1C2 (1:1000), and anti-CREB antibody (1:100). For double immunofluorescent labeling, sections were incubated with 1% sudan black B in 70% methanol for 5 minutes to block the autofluorescence.

To examine the proportion of Purkinje cells which shows different immunostaining against CREB, five random microscopic fields were selected and each immunostained Purkinje cell was classified into the following three categories; "Normal": the Purkinje cells which were stained diffusely in the cytoplasm; "Granule": the Purkinje cells containing small puncta in the cytoplasm; "Aggregate": the Purkinje cells showing thread-like structures or coarse large aggregates in the cytoplasm. The proportion of each category was calculated using the following formula: the number of Purkinje cell in each of the three groups/total number of immunostained Purkinje cells.

To examine the proportion of Purkinje cells which shows co-localization of CREB and 1C2 positive aggregates, ten consecutive Purkinje cells containing 1C2 positive aggregates in the cytoplasm was examined under a confocal laser microscope in three different regions of cerebellar cortex and calculated.

RNA isolation and real time quantitative PCR (RT-qPCR)

Total cellular RNA was isolated by TRIzol (Invitrogen, CA, USA) according to the manufactures' protocol. Cellular extracts were then treated with DNase (Invitrogen) and total RNA was quantified on a Nanodrop spectrophotometer. Total RNA was carried out reverse transcription to cDNA using a super script® III first-strand synthesis system for RT-PCR (Invitrogen) and random hexamers. The primer and probes for rCTF was designed from Life technologies (Applied biosystems by Life technologies, CA, USA). The other primer and probes were from TaqMan® Gene Expression Assays.

Statistical analysis

Where applicable, data are presented as mean ±standard error of the mean (SEM), and statistical analysis was tested by using Mann-Whitney's U test (for TUNEL assay) or a one-way analysis of variance (ANOVA) tests (all assays except for TUNEL assay). Each experiment was repeated three times independently and statistical analysis was performed.

Supporting Information

Figure S1 Presence of enhanced green fluorescent protein (EGFP) dramatically shifts the tagged rCTF into the nuclei. (A) A scheme of the recombinant $Ca_v2.1$ C-terminal fragment (rCTF) vectors with or without EGFP used in this study. (B) The rCTF-polyQ (either Q13 or Q28)-EGFP locates almost exclusively in the nuclei irrespective of the length of polyQ. This localization is quite different from the predominantly cytoplasmic location of rCTF-polyQ without EGFP. (scale bars: 50μm) (C) The proportion of the subcellular localization of each rCTF in the transiently expressing PC12 cells. (N; the cells expressing rCTF exclusively in the nucleus; N-c: the cells expressing rCTF predominantly in the nucleus than in the cytoplasm; n-C: the cells expressing rCTF

predominantly in the cytoplasm than in the nucleus; C: the cells expressing rCTF exclusively in the cytoplasm).
(PPTX)

Figure S2 rCTF expression in HEK293T cells. While rCTF-Q13 distributed both in the cytoplasm and nucleus of HEK293T cells, NLS and NES both efficiently shifted the rCTF localization in the nucleus and cytoplasm, respectively. (scale bars: 10μm).
(PPTX)

Figure S3 Co-localization of CREB and p-CREB with cytoplasmic aggregates in rCTFQ13-NES expressing PC12 cells. In PC12 cells over-expressing rCTF-Q13-NES, some of the cytoplasmic CTF aggregates co-localized with CREB (upper row) and p-CREB (lower row) (co-localizations: arrows).
(PPTX)

Acknowledgments

The authors thank Professor Hirotsugu Asahara, Dr. Kei Watase and Mr. Toshiki Unno (Tokyo Medical and Dental University) for their stimulating discussions and technical advice, Mr. Ando and Mrs. Matsuo for their excellent technical assistance, and Scientific Language Editing Team, Tsukuba, Japan, for proofreading the manuscript for editing English.

Author Contributions

Conceived and designed the experiments: KI MT. Performed the experiments: MT MO TI NS YN KO KM YM. Analyzed the data: MT KM YM H. Tanaka. Contributed reagents/materials/analysis tools: FT RD MY H. Takahashi TK OM YE. Wrote the paper: MT HM KI.

References

1. Orr HT, Zoghbi HY (2007) Trinucleotide repeat disorders. Annu Rev Neurosci 30: 575–621.
2. Shao J, Diamond MI (2007) Polyglutamine diseases: emerging concepts in pathogenesis and therapy. Hum Mol Genet 16 Spec No. 2: R115–123.
3. Zhuchenko O, Bailey J, Bonnen P, Ashizawa T, Stockton DW, et al. (1997) Autosomal dominant cerebellar ataxia (SCA6) associated with small polyglutamine expansions in the alpha 1A-voltage-dependent calcium channel. Nat Genet 15: 62–69.
4. Ishikawa K, Tanaka H, Saito M, Ohkoshi N, Fujita T, et al. (1997) Japanese families with autosomal dominant pure cerebellar ataxia map to chromosome 19p13.1-p13.2 and are strongly associated with mild CAG expansions in the spinocerebellar ataxia type 6 gene in chromosome 19p13.1. Am J Hum Genet 61: 336–346.
5. Gomez CM, Thompson RM, Gammack JT, Perlman SL, Dobyns WB, et al. (1997) Spinocerebellar ataxia type 6: gaze-evoked and vertical nystagmus, Purkinje cell degeneration, and variable age of onset. Ann Neurol 42: 933–950.
6. Ishikawa K, Fujigasaki H, Saegusa H, Ohwada K, Fujita T, et al. (1999) Abundant expression and cytoplasmic aggregations of [alpha]1A voltage-dependent calcium channel protein associated with neurodegeneration in spinocerebellar ataxia type 6. Hum Mol Genet 8: 1185–1193.
7. Matsuyama Z, Wakamori M, Mori Y, Kawakami H, Nakamura S, et al. (1999) Direct alteration of the P/Q-type Ca2+ channel property by polyglutamine expansion in spinocerebellar ataxia 6. J Neurosci 19: RC14.
8. Toru S, Murakoshi T, Ishikawa K, Saegusa H, Fujigasaki H, et al. (2000) Spinocerebellar ataxia type 6 mutation alters P-type calcium channel function. J Biol Chem 275: 10893–10898.
9. Restituito S, Thompson RM, Eliet J, Raike RS, Riedl M, et al. (2000) The polyglutamine expansion in spinocerebellar ataxia type 6 causes a beta subunit-specific enhanced activation of P/Q-type calcium channels in Xenopus oocytes. J Neurosci 20: 6394–6403.
10. Piedras-Renteria ES, Watase K, Harata N, Zhuchenko O, Zoghbi HY, et al. (2001) Increased expression of alpha 1A Ca2+ channel currents arising from expanded trinucleotide repeats in spinocerebellar ataxia type 6. J Neurosci 21: 9185–9193.
11. Saegusa H, Wakamori M, Matsuda Y, Wang J, Mori Y, et al. (2007) Properties of human Cav2.1 channel with a spinocerebellar ataxia type 6 mutation expressed in Purkinje cells. Mol Cell Neurosci 34: 261–270.
12. Watase K, Barrett CF, Miyazaki T, Ishiguro T, Ishikawa K, et al. (2008) Spinocerebellar ataxia type 6 knockin mice develop a progressive neuronal dysfunction with age-dependent accumulation of mutant CaV2.1 channels. Proc Natl Acad Sci U S A 105: 11987–11992.
13. Ishikawa K, Owada K, Ishida K, Fujigasaki H, Shun Li M, et al. (2001) Cytoplasmic and nuclear polyglutamine aggregates in SCA6 Purkinje cells. Neurology 56: 1753–1756.
14. Yabe I, Sasaki H, Matsuura T, Takada A, Wakisaka A, et al. (1998) SCA6 mutation analysis in a large cohort of the Japanese patients with late-onset pure cerebellar ataxia. J Neurol Sci 156: 89–95.
15. Takahashi H, Ishikawa K, Tsutsumi T, Fujigasaki H, Kawata A, et al. (2004) A clinical and genetic study in a large cohort of patients with spinocerebellar ataxia type 6. J Hum Genet 49: 256–264.
16. DiFiglia M, Sapp E, Chase KO, Davies SW, Bates GP, et al. (1997) Aggregation of huntingtin in neuronal intranuclear inclusions and dystrophic neurites in brain. Science 277: 1990–1993.
17. Paulson HL, Perez MK, Trottier Y, Trojanowski JQ, Subramony SH, et al. (1997) Intranuclear inclusions of expanded polyglutamine protein in spinocerebellar ataxia type 3. Neuron 19: 333–344.
18. Ishiguro T, Ishikawa K, Takahashi M, Obayashi M, Amino T, et al. (2010) The carboxy-terminal fragment of alpha(1A) calcium channel preferentially aggregates in the cytoplasm of human spinocerebellar ataxia type 6 Purkinje cells. Acta Neuropathol 119: 447–464.
19. Kordasiewicz HB, Thompson RM, Clark HB, Gomez CM (2006) C-termini of P/Q-type Ca2+ channel alpha1A subunits translocate to nuclei and promote polyglutamine-mediated toxicity. Hum Mol Genet 15: 1587–1599.
20. Li L, Saegusa H, Tanabe T (2009) Deficit of heat shock transcription factor 1-heat shock 70 kDa protein 1A axis determines the cell death vulnerability in a model of spinocerebellar ataxia type 6. Genes Cells 14: 1253–1269.
21. Marqueze-Pouey B, Martin-Moutot N, Sakkou-Norton M, Leveque C, Ji Y, et al. (2008) Toxicity and endocytosis of spinocerebellar ataxia type 6 polyglutamine domains: role of myosin IIb. Traffic 9: 1088–1100.
22. Shimohata T, Nakajima T, Yamada M, Uchida C, Onodera O, et al. (2000) Expanded polyglutamine stretches interact with TAFII130, interfering with CREB-dependent transcription. Nat Genet 26: 29–36.
23. McCampbell A, Taylor JP, Taye AA, Robitschek J, Li M, et al. (2000) CREB-binding protein sequestration by expanded polyglutamine. Hum Mol Genet 9: 2197–2202.
24. Nucifora FC, Jr., Sasaki M, Peters MF, Huang H, Cooper JK, et al. (2001) Interference by huntingtin and atrophin-1 with cbp-mediated transcription leading to cellular toxicity. Science 291: 2423–2428.
25. Milnerwood AJ, Gladding CM, Pouladi MA, Kaufman AM, Hines RM, et al. (2010) Early increase in extrasynaptic NMDA receptor signaling and expression contributes to phenotype onset in Huntington's disease mice. Neuron 65: 178–190.
26. Takahashi M, Ishikawa K, Sato N, Obayashi M, Niimi Y, et al. (2012) Reduced brain-derived neurotrophic factor (BDNF) mRNA expression and presence of BDNF-immunoreactive granules in the spinocerebellar ataxia type 6 (SCA6) cerebellum. Neuropathology. In press.
27. Jiang H, Nucifora FC, Jr., Ross CA, DeFranco DB (2003) Cell death triggered by polyglutamine-expanded huntingtin in a neuronal cell line is associated with degradation of CREB-binding protein. Hum Mol Genet 12: 1–12.
28. Li XJ (1999) The early cellular pathology of Huntington's disease. Mol Neurobiol 20: 111–124.
29. Cox LJ, Hengst U, Gurskaya NG, Lukyanov KA, Jaffrey SR (2008) Intra-axonal translation and retrograde trafficking of CREB promotes neuronal survival. Nat Cell Biol 10: 149–159.
30. Forwood JK, Lam MH, Jans DA (2001) Nuclear import of Creb and AP-1 transcription factors requires importin-beta 1 and Ran but is independent of importin-alpha. Biochemistry 40: 5208–5217.
31. Chalovich EM, Zhu JH, Caltagarone J, Bowser R, Chu CT (2006) Functional repression of cAMP response element in 6-hydroxydopamine-treated neuronal cells. J Biol Chem 281: 17870–17881.

PLOS ONE

Na^+/H^+ Exchangers Induce Autophagy in Neurons and Inhibit Polyglutamine-Induced Aggregate Formation

Kazuya Togashi[1☯¤], Shuji Wakatsuki[1☯], Akiko Furuno[1], Shinji Tokunaga[1], Yoshitaka Nagai[2], Toshiyuki Araki[1]*

1 Department of Peripheral Nervous System Research, National Institute of Neuroscience, National Center of Neurology and Psychiatry, Kodaira, Tokyo, Japan, **2** Department of Degenerative Neurological Diseases, National Institute of Neuroscience, National Center of Neurology and Psychiatry, Kodaira, Tokyo, Japan

Abstract

In polyglutamine diseases, an abnormally elongated polyglutamine results in protein misfolding and accumulation of intracellular aggregates. Autophagy is a major cellular degradative pathway responsible for eliminating unnecessary proteins, including polyglutamine aggregates. Basal autophagy constitutively occurs at low levels in cells for the performance of homeostatic function, but the regulatory mechanism for basal autophagy remains elusive. Here we show that the Na^+/H^+ exchanger (NHE) family of ion transporters affect autophagy in a neuron-like cell line (Neuro-2a cells). We showed that expression of NHE1 and NHE5 is correlated to polyglutamine accumulation levels in a cellular model of Huntington's disease, a fatal neurodegenerative disorder characterized by accumulation of polyglutamine-containing aggregate formation in the brain. Furthermore, we showed that loss of NHE5 results in increased polyglutamine accumulation in an animal model of Huntington's disease. Our data suggest that cellular pH regulation by NHE1 and NHE5 plays a role in regulating basal autophagy and thereby promotes autophagy-mediated degradation of proteins including polyglutamine aggregates.

Citation: Togashi K, Wakatsuki S, Furuno A, Tokunaga S, Nagai Y, et al. (2013) Na^+/H^+ Exchangers Induce Autophagy in Neurons and Inhibit Polyglutamine-Induced Aggregate Formation. PLoS ONE 8(11): e81313. doi:10.1371/journal.pone.0081313

Editor: *Hirofumi Arakawa, National Cancer Center Research Institute, Japan*

Received September 20, 2013; **Accepted** October 16, 2013; **Published** November 21, 2013

Funding: This study is supported by grants from the Ministry of Health, Labour, and Welfare (T.A.), and Kakenhi (19800066 and 22700407, for K.T.). The funders had no role in study design, data collection and analysis, decision to publish, or preparation of the manuscript.

Competing Interests: The authors have the following interests. Yoshitaka Nagai is a PLOS ONE Editorial Board member. This does not alter the authors' adherence to all the PLOS ONE policies on sharing data and materials.

* E-mail: taraki@ncnp.go.jp.

☯ These authors contributed equally to this work.

¤ Current address: Department of Cell Biology, Osaka Bioscience Institute, Suita, Osaka, Japan

Introduction

Accumulation and aggregation of mutant proteins is a characteristic feature of a number of neurodegenerative disorders, including Parkinson's disease and Huntington's disease (HD) [1]. In HD, for example, the disease-causing mutation in huntingtin (HTT), a protein of uncertain function causes expansion of a stretch of glutamines (polyQ) near its N terminus, and the mutant form of HTT accumulates as nuclear and cytoplasmic inclusions in an HD brain [2]. One of the major therapeutic challenges in the field of neurodegeneration has been to improve the degradation of accumulated mutant proteins.

Autophagy is a cellular protein clearance mechanism and can, in principle, clear aggregation-prone proteins [3]. In this process, double-membrane organelles, called autophagosomes, engulf cellular proteins and organelles and fuse with lysosomes to form autolysosomes, which then degrade the organelle's contents [3]. Some previous reports showed that mutated HTT expression may be associated with up-regulated autophagy, and autophagy degrades polyQ-expanded proteins [4,5].

Induction of autophagy is typically observed by nutrient deprivation in many types of cells and organs and promote protein turnover to combat against starvation [6]. The brain, on the other hand, appears to be protected against energy deprivation even when the entire body is under starvation, because nutrients (e.g., amino acids, glucose, and ketone bodies) are compensated by a constant supply from other organs. Therefore, autophagy in the brain neurons does not seem to be induced by energy deprivation, indicating that regulation of autophagy in neurons is different from that in most other cell types [7].

In this study we employed Neuro-2a cell, a neuron-like cell-line, to analyze the regulatory mechanism of autophagy. We found that the function of the Na^+/H^+ exchanger (NHE) family of ion transporters affect autophagy in Neuro-2a cells. NHEs are integral membrane proteins catalyzing the exchange of Na^+ and H^+ down their respective concentration gradients and play a role in regulating a variety of physiological processes, ranging from the fine control of intracellular pH and cell volume to systemic electrolyte, acid-base and fluid volume homeostasis [8]. Here we showed that expression of NHE1 and NHE5 is correlated to polyQ accumulation levels in cellular and animal models of HD. Together, these data suggest that cellular pH regulation by NHE1 and NHE5 play a role in regulating basal autophagy in the brain's neurons.

Materials and Methods

Animals

The technical protocols for animal experiments in this study were approved by Small Animal Welfare Committee at the National Center for Neurology and Psychiatry.

NHE5 null mutant mouse strain was obtained from Deltagen Inc. (Detailed methods and confirmation for the targeted gene deletion are provided by the company upon request.) Mice overexpressing human huntingtin residues 1–171 with 82 glutamine repeats (N171-82Q mice) [9] were obtained from the Jackson Laboratory.

Cell culture

Neuro-2a cells (ATCC) were maintained using Dulbecco's modified Eagle's medium (Invitrogen) supplemented with 10% fetal bovine serum, 25 U/ml penicillin, 25 μg/ml streptomycin (Invitrogen) and 4 mM L-glutamine (Invitrogen) in a humidifying incubator at 37 C, with 5% CO2 and 95% air, unless otherwise mentioned. Lipofectamine 2000 reagent (Invitrogen) was used for plasmid DNA transfection per manufacturer's protocol. In some experiments, cells were treated with the culture media containing 200 μM DIDS (Sigma) or 10 μM EIPA (Sigma) for 2 hr, or 10 μg/ml E64d (Peptide Institute Inc) and 10 μg/ml pepstatin A (Peptide Institute Inc) for 18 hr prior to morphological or immunoblot analysis.

Construction of expression plasmids and mutagenesis

pEGFP-C1-MAP1LC3A, pEGFP-C1-MAP1LC3B, pcDNA3-NHE1, and pcDNA3-NHE5 were constructed by amplifying coding regions of the genes by RT-PCR using total RNA extracted from mouse dorsal root ganglion neurons as a template, followed by cloning into the expression plasmids. pcDNA3-NHE1E266I and pcDNA3-NHE5E212I were generated by PCR-based mutagenesis using pcDNA3-NHE1, and pcDNA3-NHE5, respectively, as templates. For construction of dKeima-mem, EGFP region of pEGFP-C1 (Clontech) vector was replaced with dKeima-Red from pdKeima-Red-S1 (Amalgaam) and c-Ha-Ras farnesylation signal (KLNPPDESGPGCMSCKCVLS) was added to the C-terminal using a PCR-based method. NLSQ81EGFP and NESQ81EGFP plasmids were constructed by inserting nuclear localization signal sequence (PKKKRKV)or nuclear exclusion signal sequence (LALKLAGLDI) followed by human atrophin1-derived polyglutamine sequence (81 glutamine with 5 amino acid-flanking sequence derived from atrophin1 at both ends) at the multiple cloning site of pEGFP-N1 plasmid (Clontech) and a myc tag sequence at C-terminus of EGFP by a PCR-based method [10]. Expression plasmids for HttEx1-Q25-EGFP and HttEx1-Q97-EGFP were provided by Dr. A. Iwata (The University of Tokyo), and HttEx1-Q25 and HttEx1-Q97 were constructed by removing EGFP regions from them. The integrity of each clone was confirmed by sequencing.

Intracellular pH measurements

For intracellular pH estimation using dKeima-mem, fluorescence was measured in standard bath solution containing 140 mM NaCl, 5 mM KCl, 2 mM $MgCl_2$, 2 mM $CaCl_2$, 10 mM HEPES, and 10 mM glucose at pH 7.4 (adjusted with NaOH). The ratio of florescence intensities of dKeima-Red emissions at 445 nm and 586 nm was calculated for intracellular pH estimation, which was based on previous report on pH measurement using dKeima-red [11]. The high-[K+]/nigericin technique was employed to convert dKeima-Red emission intensity ratios into pH_i values [12,13]. The data shown are obtained from 961 cells in 29 independent experiments for HttEx1-Q25 expressing cells, and from 960 cells in 27 independent experiments for HttEx1-Q97 expressing cells. Differences between groups were examined for statistical significance using Welch's t-test.

For characterizing NHEs expressed in Neuro-2a cells, cells were alkalinized and acidified for 2.5 min pre-pulse technique in a solution consisting of 110 mM NaCl, 30 mM NH_4Cl, 5 mM KCl, 2 mM $CaCl_2$, 2 mM $MgCl_2$, 10 mM HEPES, 10 mM glucose at pH 7.4 (adjusted with NaOH), followed by incubation for 2.5 min in a Na^+ free solution containing 140 mM NMDG, 5 mM KCl, 2 mM $CaCl_2$, 2 mM $MgCl_2$, 10 mM HEPES, 10 mM glucose at pH 7.4 (adjusted with HCl). Recovery of intracellular pH was then observed by another 2.5 min incubation in a Na^+-containing standard bath solution. Intracellular pH change profile in a representative experiment is shown in Fig 1A. The recovery of pH_i was fitted to a single exponential function using Origin Pro 8.0 (OriginLab). "pHi recovery rate" was designated as the rate of Na^+-dependent intracellular pH (pH unit per min) at 0.05 pH_i unit increments from the point of maximum acidification. Differences between groups were examined for statistical significance using Student's t-test.

Immunofluorescence staining

NHE5 null mutant mice and their wild type littermates (9 weeks of age; 3 males for each genotype) were analyzed. Immunohistochemistry procedures were carried out as described [14]. Mouse anti-HTT a.a. 1–82 monoclonal antibody (Millipore; clone 2B4) and rabbit anti-p62/SQSTM1 polyclonal antibody (MBL) were used as primary antibodies. Alexa 488-conjugated anti-rabbit IgG, andAlexa 594-conjugated anti-mouse IgG (Molecular Probes) were used as secondary antibodies. DAPI (Sigma) was used for identification of nuclei.

Image analysis for quantification

For analysis using cultured cells, 3 images were obtained from 3 independent experiments for each condition. For aggregate quantification in brain tissues, 6 images of randomly selected fields from cerebellar cortex granular layer sections were obtained from mouse brains of indicated genotypes. Fluorescent images were captured on a laser scanning microscopy (Leica TCS SP2) using ×64 objective lens (each emage is a square, 119.047619 μm each side). Aggregate numbers were counted using PhotoshopCS4 Extended edition. Diameter of aggregate was determined by regarding that the aggregate area is circular. Differences between groups were examined for statistical significance by Student's t-test for aggregate numbers, and by Mann-Whitney's U-test for aggregate diameters.

RT-PCR analysis

For detection of mRNA expression of NHE family of molecules by RT-PCR in Neuro-2a cells, the following primer sets were used: NHE1-forward (F): CACCAGTGGAACTGGACCTT; NHE1-reverse (R): AAGGTGGTCCAGGAACTGTG; NHE2-F: CAATGACTGCCGTGAAGAGA; NHE2-R: GTCCGAGTCGCTGCTATTTC; NHE3-F CACCACAGGATTGTCCCTCT; NHE3-R: ACAGCAGGAAGGCGAAGATA; NHE4-F: GGCTTTCTCCTGAAGACGTG; NHE4-R: GTCTGTCGCCTTTCCTGAAG; NHE5-F: GCTGAGGGTGAAGAGGAGTG; NHE5-R GGCATAGAGGGCAGAGTGAG.

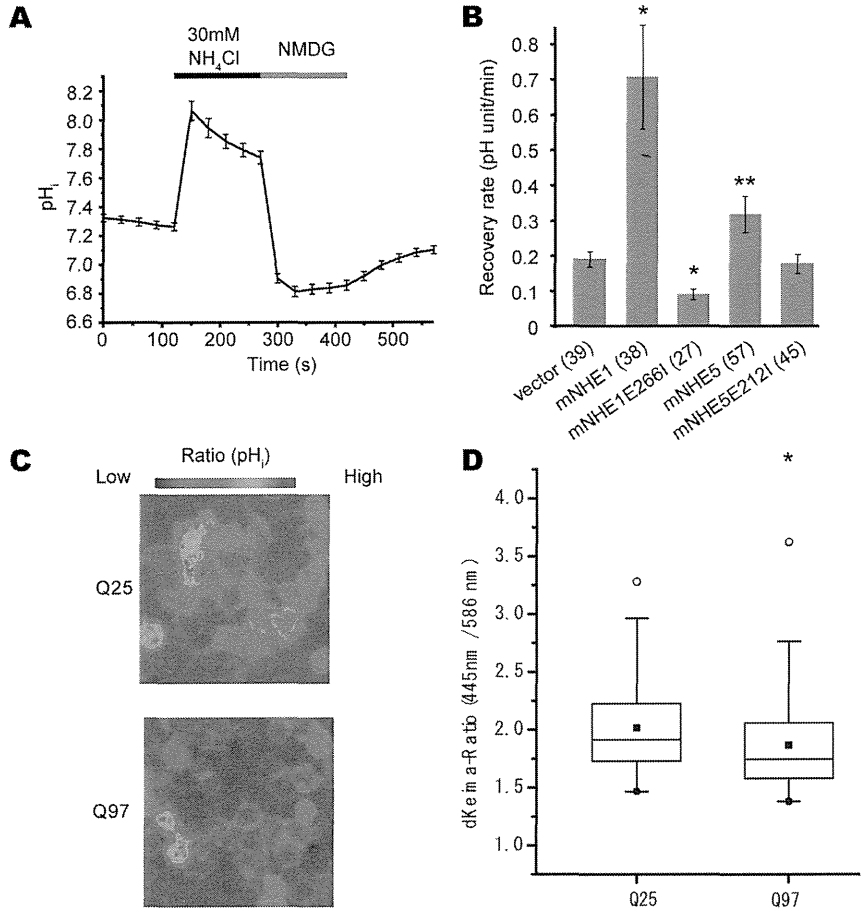

Figure 1. Acidification by polyglutamine protein expression visualized by dKeima-mem-based subcellular pH imaging. A. Representative subcellular pH imaging data in Neuro-2a cells expressing dKeima-mem during acidification followed by recovery in Na^+-free and Na^+-containing medium. B. Expression of NHE1 and NHE5 but not by their non-functional mutants facilitates recovery from acidification (see Methods). Mean pH recovery rate ±SD for each type of cells is shown as a bar graph. *P<0.01, **P<0.05 (Student's t-test; in comparison with the recovery rate of vector-only transfected control cells). Numbers in parentheses on X axis indicates the number of cells examined. C, D. Representative intracellular pH imaging results of Neuro-2a cells expressing dKeima-mem together with HttEx1-Q25 or HttEx1-Q97 demonstrated by pseudo-color images (C) and box whisker plot of quantification data 445 nm/586 nm emission ratio(D). In D, boxes represent lower quartile and upper quartile, with bars showing 1.5× of the lower and upper quartile values. White and black circles show max and min, respectively, and quadrangles show median data points. *P<0.001 (Welch's t test).
doi:10.1371/journal.pone.0081313.g001

Results

Change in extracellular pH induces autophagosome formation in the Neuro-2a cells stably expressing EGFP-LC3

Previous reports suggested that autophagy in neuronal cells is regulated in a way different from non-neuronal cells [15]. To gain insights on the mechanism of macroautophagy induction in neuron-like cells, we generated mouse neuroblastoma-derived Neuro-2a cells stably expressing EGFP-LC3 and used them as a neuron-like model system. Among physiologically relevant neuronal environmental changes that affect intracellular protein degradation, we chose to examine the effect of environmental pH changes on neuronal autophagy, because lysosomal protein degradation is heavily dependent on cellular pH regulation [16]. To modify environmental pH in cultured cells, we examined Neuro-2a cells stably expressing EGFP-LC3 maintained in an incubator with 100% air (no added CO_2) for 2 hr. We found that numbers of EGFP-positive spots were significantly increased by incubating the cells under normal air, while EGFP spot formation was not significantly affected by serum deprivation using DMEM lacking serum as culture media (FBS(−)) or by serum/amino acid-deprivation using Krebs-Ringer bicarbonate solution (KRB)(Fig. 2A). This result suggested that pH of culture environment of Neuro-2a cells affects autophagosome formation in them.

To gain insights on the mechanism of this phenomenon, we first tried to analyze which ion channels or transporters are functional in Neuro-2a cells. Major transporters implicated in intracellular pH regulation in various types of cells include sodium-hydrogen exchangers (NHEs/ SLC9 gene family) and several members of bicarbonate transporter superfamily of molecules [17]. Previous reports showed that all the known isoforms of bicarbonate-dependent transporters are inhibited by diisothiocyanostilbene disulfonic acid (DIDS) [18], while members of NHE family are inhibited by 5-(N-ethyl-N-isopropyl)-amiloride (EIPA) [19]. Therefore, we first tried these inhibitors on the Neuro-2a cells. We found that application of EIPA to the Neuro-2a cells in a 5% CO2 incubator significantly increased formation of EGFP-positive spots in the cells, while DIDS showed no effects (Fig. 2B). This result suggested that NHEs play a role in autophagosome formation in

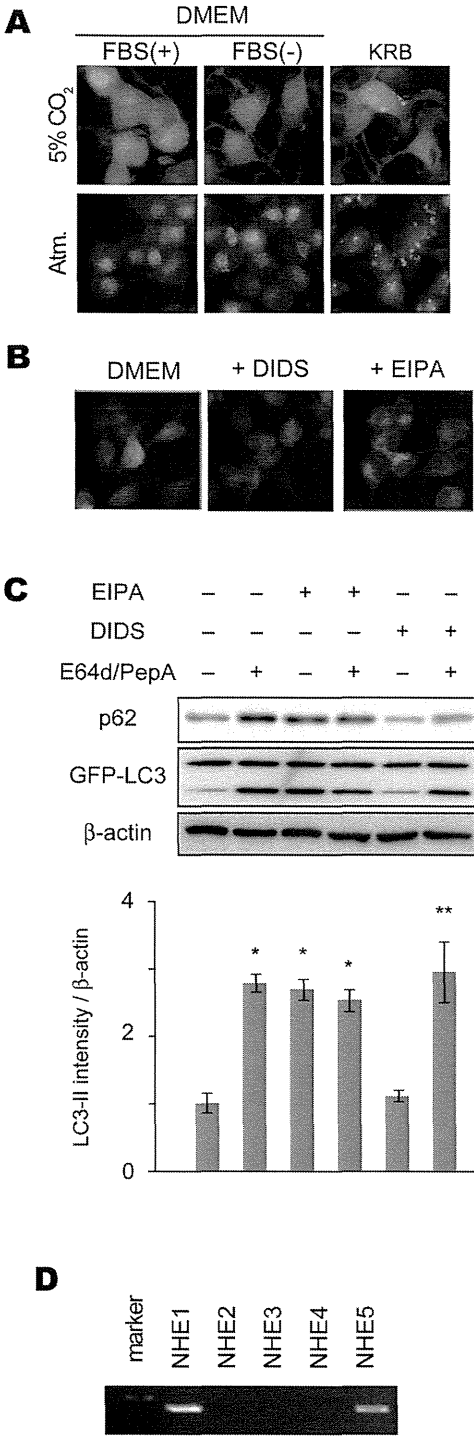

Figure 2. Neuro-2a cells show increased autophagosome formation in response to environmental pH modulation. A, B Representative photomicrographs of Neuro-2a cells stably expressing EGFP-LC3 maintained under indicated medium and atmosphere conditions for 2 hr (A), or with indicated reagents in serum-containing DMEM under 5% CO2 (B). Note the significantly increased autophagosome formation in the cells maintained in Krebs-Ringer bicarbonate buffer (KRB), which contains electrolites and glucose only under 100% normal air, and with EIPA. C Representative images of immunoblot analysis for expression of p62 and LC3 in EGFP-LC3-expressing Neuro-2a cells with indicated reagents. Bar graphs in C show quantification data of LC3-II expression levels relative to the level in EGFP-LC3-expressing Neuro-2a cells with no additional treatment normalized to β-actin expression. Results shown are mean ± SEM. *P<0.01, **P<0.05 (Student's t- test). Note that EIPA-treated cells show increased p62 and LC3-II levels indicating the inhibition of autophagic degradation by NHE inhibition. D. Detection of NHE family members in Neuro-2a cells by RT-PCR.
doi:10.1371/journal.pone.0081313.g002

the Neuro-2a cells. To distinguish whether EIPA-induced induction of autophagosome formation in Neuro-2a cells is involved in lysosomal acidification only or in induction of autophagy as well, we first performed autophagy flux assays in the presence of EIPA or DIDS (used as a negative control) [20]. We examined expression levels of p62 and LC3-I/II in Neuro-2a cells expressing GFP-LC3 in the presence of EIPA or DIDS, before and after lysosomal inhibitor (E64d/PepA) treatment. We found that EIPA treatment increased both p62 and LC3-II levels, suggesting that EIPA inhibited basal levels of autophagy in Neuro-2a cells, while DIDS did not affect the autophagy level (Fig. 2C). These results suggest that NHEs may affect autophagy levels in Neuro-2a cells. We then examined which family members of NHEs are expressed in Neuro-2a cells by RT-PCR, and found that NHE1 and NHE5 mRNA were detectable, while other members were not (Fig. 2D).

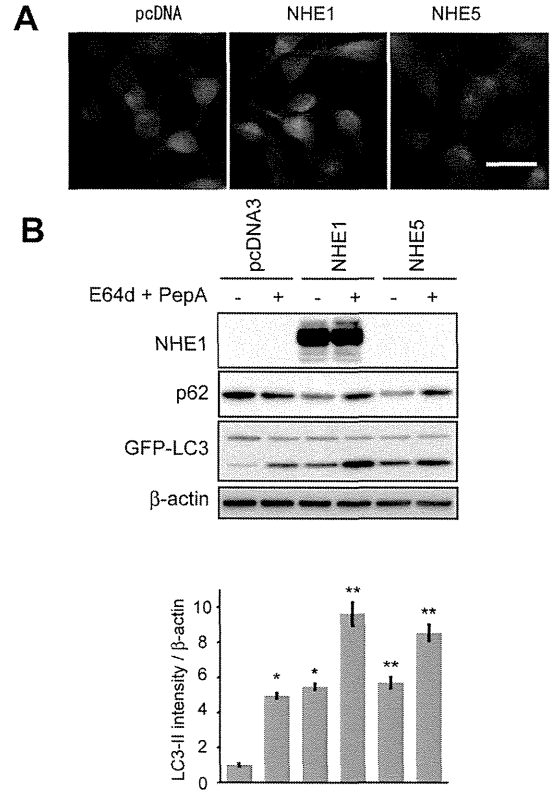

Figure 3. Induction of autophagy in Neuro-2a cells by NHE1 and NHE5. Representative photomicrographs of Neuro-2a cells stably expressing EGFP-LC3 with additional expression of NHE1 or NHE5 (A). Scale bar = 50 μm. Representative images of immunoblot analysis for expression of p62 and LC3 in EGFP-LC3-expressing Neuro-2a cells overexpressing indicated constructs (B). Bar graphs in B show quantification data of LC3-II expression levels relative to the level in EGFP-LC3-expressing Neuro-2a cells with no additional treatment normalized to β-actin expression. Results shown are mean ± SEM. *P<0.01, **P<0.05 (Student's t- test). Note that induced levels of LC3-II by overexpression of NHE1 and NHE5 was further increased by E64d/PepA, suggesting that expression of NHE1 and NHE5 induces autophagy in B.
doi:10.1371/journal.pone.0081313.g003

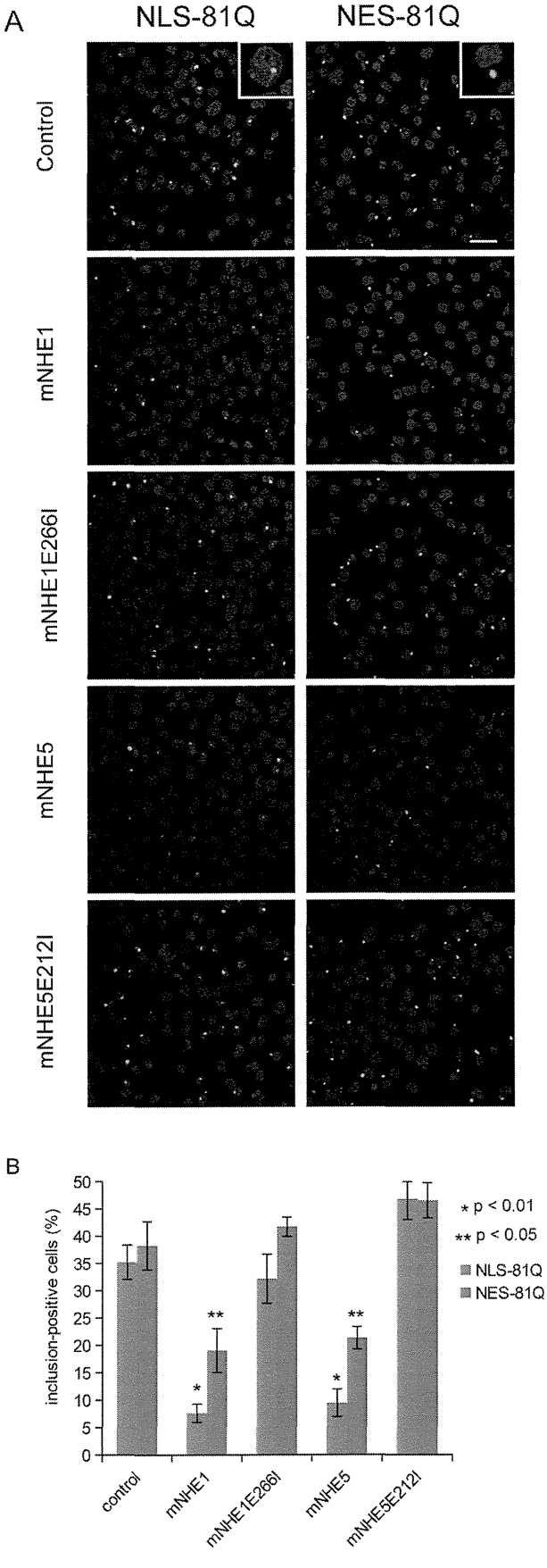

Figure 4. Expression of NHEs inhibits formation of mutant HTT aggregates. Representative photomicrographs of Neuro-2a cells overexpressing plasmids for indicated protein (A), and quantification of the aggregate-positive cell percentage (B). Insets show extranuclear and intranuclear localization of polyQ aggregates by expression of NES-81Q and NLS-81Q, respectively. Scale bar = 30 μm in (A).
doi:10.1371/journal.pone.0081313.g004

Therefore we focused the subsequent analysis on the role of NHE1 and 5.

To further characterize whether pH regulation in Neuro-2a cells by NHE1 and NHE5 is involved in induction of autophagy, we examined whether autophagy is induced in Neuro-2a cells by overexpression of NHE1 or NHE5. For this purpose, we performed autophagy flux assays under overexpression NHE1 or NHE5. To confirm that overexpressed NHE family of molecules can affect intracellular pH as expected, we introduced a pH-sensitive fluorescent dye-based imaging method by using Keima-Red with a plasma membrane localization tag (dKeima-mem). We found that this method is suitable for estimating intracellular pH around physiological level (Fig. 1). By using dKeima-mem, we were able to confirm that overexpression of NHE1 or NHE5, but not NHE1E266I or NHE5E212I, which contains a point mutation to disrupt ion transporting function of each transporter [21,22], can affect intracellular pH, suggesting that the expression constructs for NHE1 and NHE5 proteins that we used in this study are functional (Fig. 1B). To assess autophagy levels in Neuro-2a cells overexpressing NHE1 and NHE5, we employed Neuro-2a cells stably expressing EGFP-LC3 and examined morphological changes by expression of NHE1 and NHE5. We found that significantly increased number of EGFP puncta, indicative of increased autophagosome formation, by expression of NHE1 and NHE5 (Fig. 3A). We then examined changes in expression levels of LC3-I/II and p62 in Neuro-2a cells by overexpressing NHE1 or NHE5. We found that expression levels of LC3-II are increased in both types of cells (Fig. 3B). To demonstrate that this increase of LC3-II is due to induction of autophagy, we added lysosomal inhibitors (E64d and pepstatin A) to the culture of those cells. We observed an additional increase of LC3-II and p62, suggesting that expression of NHE1 or NHE5 induced autophagy (Fig. 3B). Taken together, these data suggest that NHE family of transporters, NHE1 and NHE5, may function to regulate autophagy levels in Neuro-2a cells by modulating intracellular pH.

NHE activity prevents polyQ aggregation

Wong et al. reported that expression of HTT proteins with a pathologically extended glutamine repeat in cultured cells causes acidification of culture medium [23]. Together with our current findings, we speculated that expression of abnormal polyQ protein may affect cellular autophagy by modifying intracellular pH, and thereby inhibit cellular protein degradation mechanism to cause abnormal aggregation formation. To explore this possibility, we first examined if expression of abnormally extended polyQ-containing protein changes intracellular pH by employing the dKeima-mem-based pH imaging method (see Methods for detail). We employed htt-Ex1-Q97, containing 97 stretch of glutamine chain in the first exon of HTT, as an abnormal polyQ-containing protein, and htt-Ex1-Q25 as a normal control. We overexpressed them in Neuro-2a cells together with dKeima-mem, and found that Neuro-2a cells expressing htt-Ex1-Q97 showed a relatively low 445 nm/586 nm emission rate (i.e., relatively lower pH) compared with Neuro-2a cells expressing htt-Ex1-Q25 (Fig. 1C,1D), indicating that expression of abnormal polyQ-containing protein acidifies intracellular fluid.

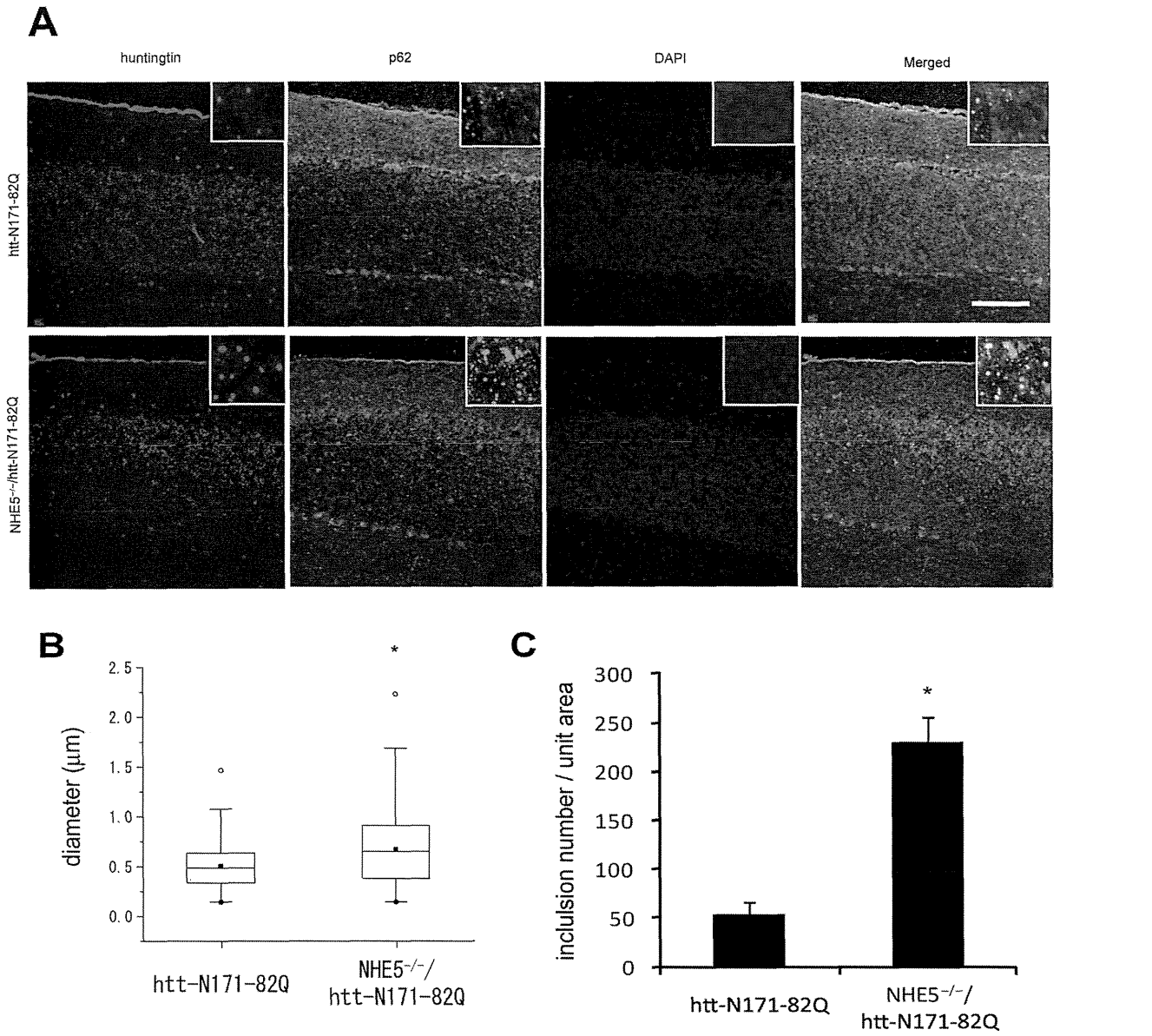

Figure 5. NHE5 null mutation increases polyglutamine protein aggregation in vivo. Representative photomicrographs of polyglutamine protein inclusions formed in cerebellar cortex of mice of the indicated genotype are shown in A. Immunoreactivity of HTT, p62, and DAPI staining images are shown with high-manification view of granular layer inclusions in insets. Scale bar = 30 μm. Quantification of the diameter (B) and number (C) of the aggregates are shown. See Method section for details. In B, boxes represent lower quartile and upper quartile, with bars showing 1.5× of the lower and upper quartile values. White and black circles show max and min, respectively, and quadrangles show median data points. *P<0.001 (Mann-Whitney's U-test). In C, data shown are mean ± SD. *P<0.05(Student's t-test).
doi:10.1371/journal.pone.0081313.g005

To know whether NHE expression affects intracellular polyQ aggregation status, we examined aggregation of polyQ in Neuro-2a cells with or without co-expression of NHE1 or NHE5. PolyQ aggregates are often formed in nuclei, while autophagy-mediated protein degradation occurs in cytoplasm [2]. Therefore, in this experiment, we employed cytoplasmic (NESQ81EGFP-myc) and nuclear polyQ protein (NLSQ81EGFP-myc) expression constructs to examine how expression of NHEs affect the polyQ aggregation derived from each of these constructs. We found that expression of NHE1 or NHE5 suppressed formation of EGFP-labeled polyQ aggregation in cytoplasm and nucleus, while expression of mutant forms of NHE1 and NHE5 did not (Fig. 4). These results suggest that expression of NHE1 and NHE5 function to inhibit polyQ aggregate formation by increasing autophagic degradation of cytoplasmic protein aggregates, which may affect the global polyQ metabolism to decrease nuclear aggregations as well.

To examine the roles of NHEs in more physiological settings, we employed a mouse model polyQ aggregation and examined how it is affected by NHE expression. To this end, we crossed N171-82Q mice (HD model mice overexpressing N-terminal fragment of HTT containing 82 glutamine repeats) with NHE5 knock-out mice. NHE5 knockout mice were generated by insertion of neo-resistance cassette in the exon 6 of mouse NHE5 gene. NHE5 null mutant mice were born with expected Mendelian frequency and did not show gross defect, developmental abnormality, or reproductive failure (data not shown). N171-82Q mice

develop nuclear inclusion of mutant HTT in many regions of the brain [9]. To examine the effect of NHE5 deletion in polyQ accumulation in the brain of N171-82Q mice, we examined immunohistochemical distribution of polyQ aggregation in N171-82Q mouse cerebellum with NHE5-null background. From randomly acquired fields, the entire granular layer (from the region right next to the Pukinje cells to medulla) was evaluated for the formation of polyQ aggregation. We found that N171-82Q mouse cerebellar tissues with NHE5-null background showed increased size and numbers of nuclear inclusions (Fig. 5). These data suggest that NHE5 functions to promote degradation of abnormal proteins including polyQ by activating autophagy.

Discussion

In the current study, we demonstrated that NHEs play a role in maintaining normal neuronal functionality by regulating intracellular pH, and thereby promoting autophagy-mediated degradation of proteins including polyQ-containing molecules. NHE-mediated cellular pH maintenance seemed to contribute to the regulation of basal autophagy levels in neuronal cells. In N171-82Q /NHE5KO mouse cerebellum, we found an increase of polyglutamine aggregation mostly in nuclei of neurons. Previous reports showed that induction of autophagy-mediated protein degradation promotes clearance of cytoplasmic but not nuclear aggregates [3]. However, it is also reported that RNAi-mediated reduction of autophagy machinery may result in a slight increase of nuclear inclusions as well [24]. Our current data suggest that by promoting autophagy-mediated degradation of cytoplasmic aggregation of polyQ, nuclear inclusion can be reduced as well. It is also possible that NHE5 expression may affect other protein degradation system such as the ubiquitin-proteasome system to increase degradation of nuclear inclusions. Further studies will be necessary to explore this possibility.

In this work, we employed NHE5 null-mutant mice to examine *in vivo* role of NHEs in degradation of polyQ, because NHE1 null mutation causes severe developmental defects, including ataxia, growth retardation, and seizures, and results in high mortality rate in early postnatal development [25,26]. In our experiments using Neuro-2a cell culture, we found both NHE1 and NHE5 show equivalent effect in inducing autophagy, suggesting that NHE1 may also function to promote degradation of polyQ aggregates. To prove this possibility using mouse models, NHE1 conditional KO mice that lack NHE1 in limited regions such as postmitotic neurons may be necessary.

Thus far, it is not clear how the change in cytoplasmic pH induces basal autophagy in neurons. Because intracellular pH is affected by cellular energy production/consumption and metabolic stresses [27], and metabolic changes are key regulators of autophagy [3], it is possible that NHE-induced regulation of autophagy is mediated by a signaling mechanism similar to the regulatory mechanism of energy deprivation-induced autophagy. It is also possible that another novel regulatory mechanism is involved in NHE-induced autophagy, because NHEs affect basal levels of autophagy, which is often regarded as one regulated under a mechanism different from energy deprivation-induced autophagy [3]. Further studies will need to be done to fill the gap between cellular pH regulation and changes in basal autophagy status.

Acknowledgments

The authors would like to thank Dr. A. Iwata for HttEx1-Q25-EGFP and HttEx1-Q97-EGFP plasmids, Dr H.A. Popiel for technical assistance, and all the members of our laboratory for many helpful discussions.

Author Contributions

Conceived and designed the experiments: KT SW TA. Performed the experiments: KT SW AF. Analyzed the data: KT SW AF ST. Contributed reagents/materials/analysis tools: KT SW AF ST YN. Wrote the paper: KT TA.

References

1. Moreno-Gonzalez I, Soto C (2011) Misfolded protein aggregates: mechanisms, structures and potential for disease transmission. Semin Cell Dev Biol 22: 482–487.
2. Ross CA, Tabrizi SJ (2011) Huntington's disease: from molecular pathogenesis to clinical treatment. Lancet Neurol 10: 83–98.
3. Mizushima N, Komatsu M (2011) Autophagy: renovation of cells and tissues. Cell 147: 728–741.
4. Choi AM, Ryter SW, Levine B (2013) Autophagy in human health and disease. N Engl J Med 368: 651–662.
5. Rubinsztein DC (2006) The roles of intracellular protein-degradation pathways in neurodegeneration. Nature 443: 780–786.
6. Nakatogawa H, Suzuki K, Kamada Y, Ohsumi Y (2009) Dynamics and diversity in autophagy mechanisms: lessons from yeast. Nat Rev Mol Cell Biol 10: 458–467.
7. Xie Z, Klionsky DJ (2007) Autophagosome formation: core machinery and adaptations. Nat Cell Biol 9: 1102–1109.
8. Orlowski J, Grinstein S (2004) Diversity of the mammalian sodium/proton exchanger SLC9 gene family. Eur J Physiol 447: 549–565.
9. Schilling G, Becher MW, Sharp AH, Jinnah HA, Duan K, et al. (1999) Intranuclear inclusions and neuritic aggregates in transgenic mice expressing a mutant N-terminal fragment of huntingtin. Hum Mol Genet 8: 397–407.
10. Nagai Y, Tucker T, Ren H, Kenan DJ, Henderson BS, et al. (2000) Inhibition of polyglutamine protein aggregation and cell death by novel peptides identified by phage display screening. J Biol Chem 275: 10437–10442.
11. Katayama H, Kogure T, Mizushima N, Yoshimori T, Miyawaki A (2011) A sensitive and quantitative technique for detecting autophagic events based on lysosomal delivery. Chem Biol 18: 1042–1052.
12. Fujita F, Uchida K, Moriyama T, Shima A, Shibasaki K, et al. (2008) Intracellular alkalization causes pain sensation through activation of TRPA1 in mice. J Clin Invest 118: 4049–4057.
13. Thomas JA, Buchsbaum RN, Zimniak A, Racker E (1979) Intracellular pH measurements in Ehrlich ascites tumor cells utilizing spectroscopic probes generated in situ. Biochemistry 18: 2210–228.
14. Togashi K, Hara Y, Tominaga T, Higashi T, Konishi Y, et al. (2006) TRPM2 activation by cyclic ADP-ribose at body temperature is involved in insulin secretion. Embo J 25: 1804–1815.
15. Mizushima N, Yamamoto A, Matsui M, Yoshimori T, Ohsumi Y (2004) In vivo analysis of autophagy in response to nutrient starvation using transgenic mice expressing a fluorescent autophagosome marker. Mol Biol Cell 15: 1101–1111.
16. Shintani T, Klionsky DJ (2004) Autophagy in health and disease: a double-edged sword. Science 306: 990–995.
17. Taylor CJ, Nicola PA, Wang S, Barrand MA, Hladky SB (2006) Transporters involved in regulation of intracellular pH in primary cultured rat brain endothelial cells. J Physiol 576: 769–785.
18. Wulff H (2008) New light on the "old" chloride channel blocker DIDS. ACS Chem Biol 3: 399–401.
19. Masereel B, Pochet L, Laeckmann D (2003) An overview of inhibitors of Na(+)/H(+) exchanger. Eur J Med Chem 38: 547–554.
20. Klionsky DJ, Abdalla FC, Abeliovich H, Abraham RT, Acevedo-Arozena A, et al. (2012) Guidelines for the use and interpretation of assays for monitoring autophagy. Autophagy 8: 445–544.
21. Denker SP, Huang DC, Orlowski J, Furthmayr H, Barber DL (2000) Direct binding of the Na--H exchanger NHE1 to ERM proteins regulates the cortical cytoskeleton and cell shape independently of H(+) translocation. Mol Cell 6: 1425–1436.
22. Diering GH, Mills F, Bamji SX, Numata M (2011) Regulation of dendritic spine growth through activity-dependent recruitment of the brain-enriched Na(+)/H(+) exchanger NHE5. Mol Biol Cell 22: 2246–2257.
23. Wong HK, Bauer PO, Kurosawa M, Goswami A, Washizu C, et al. (2008) Blocking acid-sensing ion channel 1 alleviates Huntington's disease pathology via an ubiquitin-proteasome system-dependent mechanism. Hum Mol Genet 17: 3223–3235.
24. Iwata A, Christianson JC, Bucci M, Ellerby LM, Nukina N, et al. (2005) Increased susceptibility of cytoplasmic over nuclear polyglutamine aggregates to autophagic degradation. Proc Natl Acad Sci U S A 102: 13135–13140.

25. Bell SM, Schreiner CM, Schultheis PJ, Miller ML, Evans RL, et al. (1999) Targeted disruption of the murine Nhe1 locus induces ataxia, growth retardation, and seizures. Am J Physiol 276: C788–795.
26. Cox GA, Lutz CM, Yang CL, Biemesderfer D, Bronson RT, et al. (1997) Sodium/hydrogen exchanger gene defect in slow-wave epilepsy mutant mice. Cell 91: 139–148.
27. Pedersen SF, O'Donnell ME, Anderson SE, Cala PM (2006) Physiology and pathophysiology of Na+/H+ exchange and Na+ -K+ -2Cl- cotransport in the heart, brain, and blood. Am J Physiol Regul Integr Comp Physiol 291: R1–25.

Journal of Neurochemistry JNC

JOURNAL OF NEUROCHEMISTRY | 2013 | 126 | 288–300 doi: 10.1111/jnc.12194

ORIGINAL ARTICLE

TDP-43 associates with stalled ribosomes and contributes to cell survival during cellular stress

Shinji Higashi,*† Tomohiro Kabuta,* Yoshitaka Nagai,* Yukihiro Tsuchiya,* Haruhiko Akiyama† and Keiji Wada*

*Department of Degenerative Neurological Diseases, National Institute of Neuroscience, National Center of Neurology and Psychiatry, Tokyo, Japan

†Dementia Project, Department of Dementia and Higher Brain Function, Tokyo Metropolitan Institute of Medical Science, Tokyo, Japan

Abstract

TAR DNA-binding protein 43 (TDP-43) has emerged as an important contributor to amyotrophic lateral sclerosis and frontotemporal lobar degeneration. To understand the physiological roles of TDP-43 in the complex translational regulation mechanisms, we exposed cultured cells to oxidative stress induced by sodium arsenite (ARS) for different periods of time, leading to non-lethal or sublethal injury. Polysome profile analysis revealed that ARS-induced stress caused the association of TDP-43 with stalled ribosomes via binding to mRNA, which was not found under the steady-state condition. When the cells were exposed to short-term/non-lethal stress, TDP-43 associating with ribosomes localized to stress granules (SGs); this association was transient because it was immediately dissolved by the removal of the stress. In contrast, when the cells were exposed to long-term/sublethal stress, TDP-43 was excluded from SGs and shifted to the heavy fractions independent of any binding to mRNA. In these severely stressed cells, biochemical alterations of TDP-43, such as increased insolubility and disulfide bond formation, were irreversible. TDP-43 was finally phosphorylated via the ARS-induced c-jun N-terminal kinase pathway. In TDP-43-silenced cells, stalled mRNA and poly $(A)^+$ RNA stability was disturbed and cytotoxicity increased under sublethal stress. Thus, TDP-43 associates with stalled ribosomes and contributes to cell survival during cellular stress.

Keywords: amyotrophic lateral sclerosis, apoptosis, frontotemporal lobar degeneration, oxidative stress, stress granule, TDP-43.

J. Neurochem. (2013) **126**, 288–300.

Amyotrophic lateral sclerosis (ALS) is a fatal neurodegenerative disease characterized by the relentless degeneration of both upper and lower motor neurons and the presence of intraneuronal aggregates in the affected tissue. Although the exact mechanisms underlying ALS remain unclear, both genetic predisposition and environmental risk factors are thought to contribute to the development of the disease. In addition to increasing age, several potential environmental stresses, including oxidative stress, mitochondrial dysfunction, excitotoxicity, and endoplasmic reticulum stress, are speculated to be involved in the disease (Cleveland and Rothstein 2001; Bruijn *et al.* 2004). However, it has not been elucidated which of the processes involved in the stress response is the most important for triggering cell death in the disease.

Recently, two genes encoding DNA/RNA-binding proteins, TAR DNA-binding protein 43 (TDP-43) and fused in sarcoma/translated in liposarcoma (FUS/TLS, hereafter referred to as FUS), were reported to be ambiguous causes of FALS (Kabashi *et al.* 2008; Sreedharan *et al.* 2008; Kwiatkowski *et al.* 2009; Vance *et al.* 2009). These proteins have structural and functional similarities, including an RNA-recognition motif and a glycine-rich region, and belong to the group of heterogeneous nuclear ribonucleoproteins (hnRNPs). Moreover, TDP-43 and FUS are major components of proteinaceous inclusions observed in affected regions from patients with sporadic ALS or frontotemporal lobar degeneration (FTLD) (Arai *et al.* 2006; Neumann *et al.* 2006). Thus, the RNA metabolism that these proteins are

Received August 23, 2012; revised manuscript received February 5, 2013; accepted February 6, 2013.

Address correspondence and reprint requests to Shinji Higashi, MD, PhD, Dementia Project, Department of Dementia and Higher Brain Function, Tokyo Metropolitan Institute of Medical Science, 2-1-6 Kamikitazawa, Setagaya-ku, Tokyo 156-0057, Japan.
E-mail: higashi-sj@igakuken.or.jp

Abbreviations used: ALS, amyotrophic lateral sclerosis; ARS, sodium arsenite; FTLD, frontotemporal lobar degeneration; SARK, sarkosyl; SG, stress granule; TDP-43, TAR DNA-binding protein 43.

involved in may be central to the pathogenesis of ALS and FTLD. Intriguingly, under diverse stress conditions, TDP-43 and FUS proteins are reported to localize to stress granules (SGs), cytoplasmic messenger ribonucleoproteins (mRNPs) in which non-translating mRNA, many translation initiation components and RNA-binding proteins accumulate (Colombrita *et al.* 2009; Liu-Yesucevitz *et al.* 2010; Dewey *et al.* 2011; McDonald *et al.* 2011; Meyerowitz *et al.* 2011). These stresses inducing SGs limit protein synthesis, mostly via inhibition of translation initiation (Anderson and Kedersha 2009). mRNA translation and stability in SGs may play important roles in determining cell fate during stress. Mild or intermediate stress causes the recovery of translation and the synthesis of proteins essential for adaptation followed by cell survival. However, prolonged or severe stress promotes cell death, mostly via inducing apoptosis. In fact, SGs harbor several apoptosis regulatory factors and affect cell survival rates following exposure to stress (Buchan and Parker 2009). Thus, the cellular response to stress involves regulation of mRNA translation, for example, the synthesis of pro-survival or pro-apoptotic proteins. However, the exact nature of this mechanism in affected brain regions from patients with ALS or FTLD remains unresolved. Therefore, identifying pathological alterations of mRNA metabolism occurring in these diseases will provide important insights into the pathogenesis of these diseases.

In this study, we examined the physiological roles of TDP-43 in the complex translational regulation mechanisms determining cell fate under conditions of oxidative stress. Under oxidative stress induced by sodium arsenite (ARS), which induces cells to assemble cytoplasmic stress granules (SGs), multimolecular aggregates of stalled translation preinitiation complexes that prevent the accumulation of misfolded proteins (Arimoto *et al.* 2008), we found that TDP-43 associated with stalled ribosomes, and appears to play an important role(s) in mRNA stability and cell survival.

Methods

Cell culture, transfection, plasmids, reagents, antibodies, Western blotting, immunocytochemistry, RNAi experiments, and quantitative assessment of cell death

Detailed procedures are described in the previous study (Higashi *et al.* 2010) and the Supplemental methods.

Polysome profile analysis by linear sucrose gradient fractionation

Polysome profile analysis was carried out as previously described (Kawai *et al.* 2004; Lu *et al.* 2009) with minor modifications. HeLa cells were grown in 10-cm dishes to about 80% confluence. After some treatments with ARS, cells were cultured in medium with 0.1 mg/mL cycloheximide (Sigma-Aldrich, St. Louis, MO, USA) at 37°C for 3 min for analysis of polyribosomes as previously described (Feng *et al.* 1997). Cells were washed twice with cold phosphate-buffered saline (PBS) containing 0.1 mg/mL cycloheximide, and then lysed in polysome lysis buffer containing 15 mM Tris-HCl, pH 8.0, 300 mM NaCl, 15 mM $MgCl_2$, 1% Triton X-100, 1 mg/mL heparin and 0.1 mg/mL cycloheximide on ice for 10 min. Lysates were centrifuged at 10 000 *g* for 10 min. For the RNase experiments, prior to ultracentrifugation, lysates were treated with 300 μg/mL RNase A at 30°C for 15 min as previously described (Ceman *et al.* 2003). For fractionation, a total of 1 mL of the supernatant obtained from three 10-cm dishes was loaded onto 10 mL of 10–50% sucrose gradients containing 15 mM Tris-HCl, pH 8.0, 300 mM NaCl, 5 mM $MgCl_2$, 0.5 mg/mL heparin, 0.1 mg/mL cycloheximide in Ultra-Clear Centrifuge Tubes (14 × 89 mm, Beckman, Palo Alto, CA, USA), and separated by ultracentrifugation with a SW41 rotor (Beckman) at 35 000 rpm at 4°C for 90 min. Each gradient was collected into 1-mL fractions from bottom with the ribosomal profile monitored by absorbance measurements at 260 nm (Atto, Tokyo, Japan). Equal volumes from each fraction were used for Western blotting.

Fluorescence *in situ* hybridization

Control or TDP-43-silenced SH-SY5Y cells were prepared in six-well plates as described in the Supplementary Methods section. After incubation with reagent, cells were rinsed with TBS, fixed with 4% paraformaldehyde for 10 min, permeabilized with 100% methanol for 10 min at −20°C, and then rehydrated for 1 h at 4°C with 70% ethanol. After incubation in 1 M Tris-HCl (pH 8.0) for 5 min at 22°C, cells were hybridized overnight at 37°C with 1 μg/mL Cy™3-oligo-dT(30) in hybridization buffer (1 mg/mL yeast tRNA, 0.005% bovine serum albumin , 10% dextran sulfate, 25% deionized formamide, 2 × SSC). After washing, sections were incubated for 3 h with anti-TDP-43 antibody at a 1 : 200 dilution in 0.1% Triton X-100 in 2 × SSC at 22°C. After further washing, sections were incubated for 2 h with Cy™2-conjugated secondary antibody (Jackson ImmunoResearch Lab, Inc., Baltimoer Pike, PO) at a 1 : 200 dilution in 0.1% Triton X-100 in 2 × SSC at 22°C. After incubating with 4′, 6-diamidino-2-phenylindole (DAPI) for 2 min, the cover slips were washed and mounted in mounting medium. Mean fluorescence intensity per cell in each siRNA-transfected cell was calculated from three independent experiments using Zeiss LSM ZEN 2010 software (Carl Zeis MicroImaging GmbH, Jena, Germany) according to the manufacturer's instructions.

Results

TDP-43 associates with stalled ribosomes under oxidative stress

To understand the physiological roles of TDP-43 in translational regulation, we conducted polysome profile analysis in HeLa cells treated with ARS. After treatment with cycloheximide to trap elongating ribosomes, HeLa cells were lysed with polysome lysis buffer containing Triton X-100 and heparin to extract membrane-bound polysomes and stabilize RNA (Gauthier and Ven Murthy 1987) and then fractionated on a 10–50% sucrose density gradient. Ultracentrifugation allowed separation of the ribosomal subunits and polysome profiles were then obtained by absorbance measurements at 260 nm during fraction collection.

The polysome profile under the steady-state condition, including peaks for the 40S and 60S ribosomal subunits, 80S

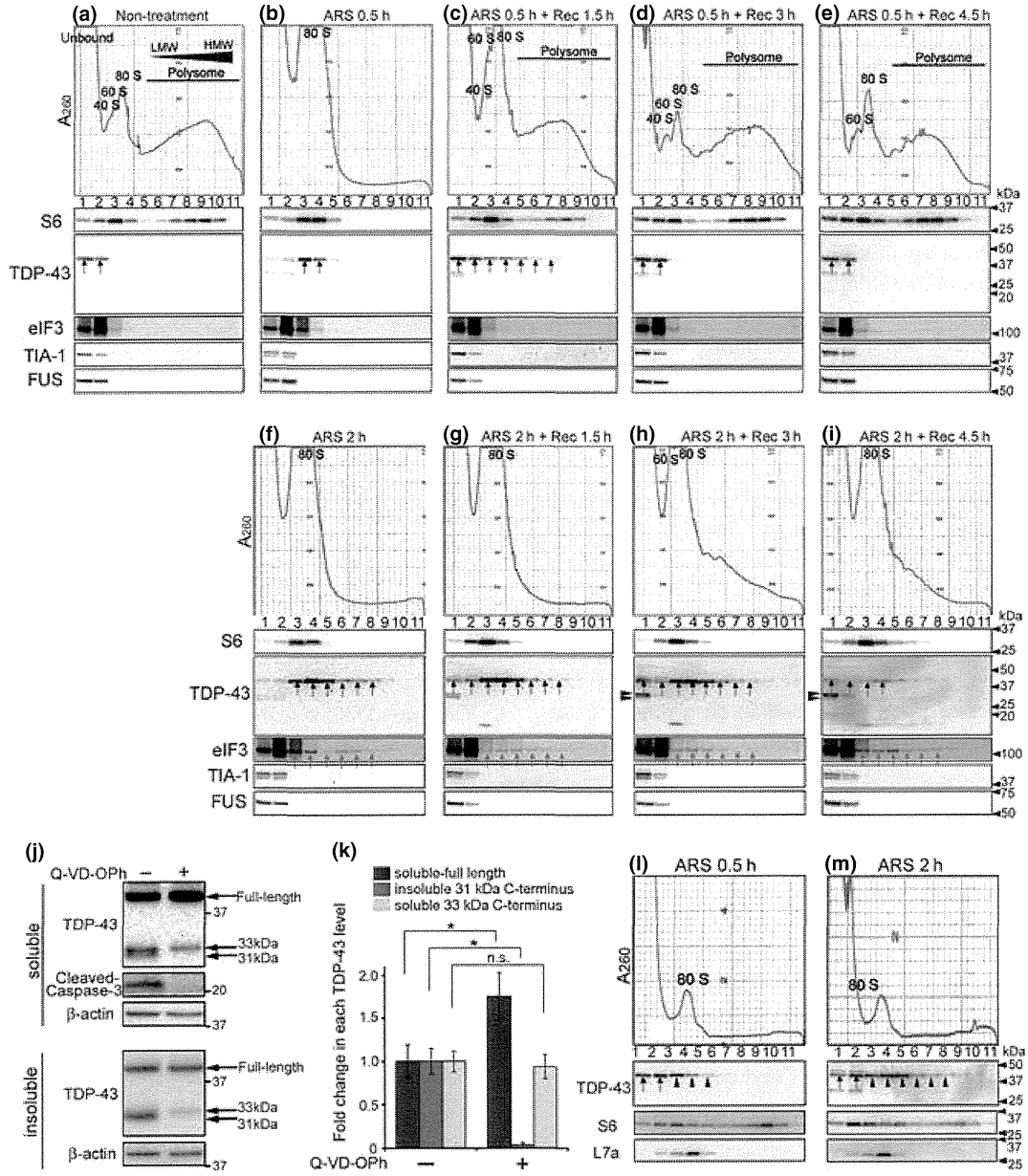

monosomes and actively translating polysomes, is indicated in Fig. 1a. The 40S ribosomal protein S6 co-fractionated with the major monosome (Fig. 1a fractions 2–4) or polysome (Fig. 1a fractions 6–10). Under this normal condition, TDP-43 was found in fractions of lower density devoid of ribosomes (Fig. 1a fractions 1 and 2). Other SG-associated RNA-binding proteins, namely, TIA-1, FUS (Fig. 1a), HuR, and G3BP1 (data not shown), also remained in the non-ribosomal fraction, while eIF3 was partially fractionated to the 40S ribosomal fraction as previously reported (Kedersha *et al.* 2002) (Fig. 1a fraction 3). Previous studies have reported that TDP-43 is incorporated into SGs in response to several stress stimuli (Colombrita *et al.* 2009; Liu-Yesucevitz *et al.* 2010; Dewey *et al.* 2011; McDonald *et al.* 2011; Meyerowitz *et al.* 2011). To characterize the molecular properties of TDP-43 under the stress condition, we treated cells with ARS, which induces oxidative stress followed by formation of SGs. ARS treatment for 0.5 h induced dissociation of polysomes and a shift of S6 to the high monosomal peak, suggesting that the monosomal peak includes some SG components, such as stalled ribosomes and mRNAs (Fig. 1b fractions 3 and 4). In fact, this treatment induced formation of SGs in which TIA-1 and S6 were co-localized (Fig. 2b and g). In these treated cells, TDP-43 and some eIF3 were fractionated to the monosomal fractions from the non-ribosomal fractions (Fig. 1b fractions 3 and 4), while FUS, TIA-1, HuR, and G3BP1 remained in fractions at the top of the gradients (Fig. 1b and data not shown). Thus, TDP-43 not only localized to SGs (Fig. 2g) but also was able to